SRC-I Quarterly Technica Report

January–March 1980

International Coal Refining Company

Allentown, Pennsylvania

DISCLAIMER

SRC-I QUARTERLY TECHNICAL REPORT

JANUARY—MARCH 1980

SRC-I
Solvent-Refined Coal

QUARTERLY

TECHNICAL

REPORT

JANUARY—MARCH 1980

by

INTERNATIONAL COAL REFINING COMPANY
P. O. Box 2752, Allentown, PA 18001

to

UNITED STATES DEPARTMENT OF ENERGY
Division of Energy Technology
under Contract DE-AC05-78-ORO-3054

TABLE OF CONTENTS

TESTING THE NARA PADDLE DRYER TO REDUCE DEASHING SOLVENT LEVELS

S. Venkat Raman*

As a result of the unsatisfactory performance of the ash concentrate dryer at Wilsonville, high levels of deashing solvent (1 to 10 wt %) have been reported in the ash concentrate. Levels below 1 wt % are desired. In fact, specific ash handling and transport procedures may dictate that the deashing solvent be reduced to trace amounts.

The Phase 0 design for the ash concentrate dryer is similar to that at Wilsonville, i.e., a flash drum with a steam stripper. Equipment modifications are under way at Wilsonville to demonstrate the operation of the flash drum-steam stripper and obtain data on the fines carryover.

If, after the modifications, the deashing solvent content is still too high, a dryer with a long residence time will be required downstream of the flash drum. In order to have this option available if the need arises, ICRC is conducting tests of drying Kerr-McGee ash concentrate from Wilsonville in such a dryer, a Nara Paddle Dryer.

THE NARA PADDLE DRYER

The Nara Paddle Dryer consists of a long, jacketed trough in which the granular material to be dried is agitated by revolving, hollow, cuneiform paddles (see Figure 1). Heat transfer fluid may be circulated through the jacket and the hollow paddles. Different models are available for use with liquid or vapor heat transfer media. Many closely spaced paddles are mounted on hollow shafts running the length of the trough. There are either two or four shafts to a dryer. A large ratio of heat transfer, surface to volume, is achieved in this manner.

The feed and discharge of material are through rotary airlock valves. The flow of material through the dryer is by gravity and, to facilitate this flow, the unit is mounted on a slight gradient. Carrier gas sweeps away the evaporated solvent. However, the solvent may be recovered and the gas recycled, if desired.

The paddle revolution rate is kept low, usually 10-40 rpm, to minimize erosion of dryer surfaces and particle attrition.

Preliminary drying tests were done at various temperatures in a laboratory oven at Air Products and Chemicals, Inc. (APCI), and in a Nara paddle dryer test unit located at the test center of Stork-Bowen Engineering (S-B), Somerville, NJ. These tests indicated that rapid drying occurs at temperatures above 300°F and established the flowability of the material through the Nara dryer.

*ICRC

A demonstration of continuous ash concentrate drying on a Nara dryer was conducted at the manufacturer's facilities in Tokyo. The heating medium was 100 psig saturated steam (338°F) and the space above the bed of solids was purged with hot nitrogen to avoid oxidation of the material. In the test, the deashing solvent levels in the ash concentrate were reduced from 2 wt % to 0.05 wt %.

Additional testing is planned at the S-B test center to optimize operating variables and to quantify fines carryover in the purge nitrogen stream and the particle size distribution.

On the basis of this information, a particulate removal and solvent recovery system will be designed to go with the dryer for possible installation at Wilsonville.

DISCUSSION

Preliminary Drying Tests. These tests were done on K-M ash concentrate from Wilsonville (Run No. 167-86, 28 August 1979), containing 2.8 wt % residual solvent.

A batch drying test was conducted at the S-B test center on a Nara pilot unit using 15 psig saturated steam, with the top cover of the unit removed. Samples were collected every 3 to 5 minutes for 35 minutes. The maximum temperature attained in the bed was 228°F. Samples were analyzed for deashing solvent by extraction with ethyl alcohol followed by gas chromatography. After 35 minutes drying time, the deashing solvent level in the ash concentrate was 0.9 wt %.

When this test was done (28 September 1979), S-B had not yet installed air lock valves on their Nara unit and the material could not be isolated from the atmosphere by purging with inert gas. This made it impossible to run tests on the S-B equipment at higher temperatures, the material being pyrophoric—arrangements were made for a demonstration test at Nara Machinery Company, Ltd., Tokyo.

Meanwhile, drying tests were done in a laboratory dryer that was continuously purged with nitrogen. The tests were conducted at 250, 300 and 350°F by placing 5-10 gram samples in shallow dishes in the oven, removing them at various intervals up to 3 hours, and analyzing for deashing solvent. The results indicate rapid drying at 300°F and above (see Table 1). On this basis it was decided that the Tokyo demonstration test would be done at 300°F.

Nara Demonstration Test. A demonstration of K-M ash concentrate drying on the Nara unit was conducted on 11 January 1980 at Tokyo. The test unit was a Nara Paddle Dryer, Model NPD 1.6W, pilot scale unit. The trough is about 6 ft long, 1 ft wide, and 7 inches deep. It has two shafts with paddles approximately 6 inches in diameter. The usable bed volume is about 2 ft^3 and the total heat transfer area is 27 ft^2 (see flowsheet of the test unit in Figure 2).

Saturated steam at 7 kg/cm^2 (100 psig, 338°F) was applied to the jacket and the paddle shafts. A stream of nitrogen (300 liters/min) was heated to 260°F by means of an electric heater and passed once through the dryer, countercurrent to the flow of ash and vented to a hood. Ash concentrate (Wilsonville Run No. 172 A and B, 1 October 1979) was fed to the unit through a hopper at the rate of 2 lb/min and dried product was discharged through a rotary air lock valve. The unit was inclined at 2° to permit the flow of solids along the length of the dryer.

The temperatures of the steam, nitrogen (inlet), and the ash at four points along the length of the dryer were continuously recorded.

The dryer was warmed by applying steam to the jacket and paddle shafts, and purged with hot nitrogen for 45 minutes before ash concentrate was fed to the unit.

The first discharge of material from the dryer started approximately 30 minutes after commencement of feed to the unit. All temperatures reached a steady state 75 minutes after the start of feed.

Samples of material were collected at six points along the length of the dryer after 90 minutes from start of feed. In addition, feed and product samples were also collected.

Nara Machinery determined the "moisture" content of samples by weight loss on drying the samples in a vacuum oven at 300 mm Hg and 250°F for five hours. The deashing solvent content of samples was determined at APCI.

While the total moisture content of the ash concentrate decreased from 17 wt % to 0.15 wt %, the deashing solvent content decreased from 2 wt % to 0.05 wt % in one pass through the dryer (see Figure 3).

A Karl-Fischer water analysis was performed on samples of the starting and dried ash concentrate by APCI. The water content of the starting material ranged from 15 to 21 wt % and that of the dried material was about uniform at 0.2 wt %. This data clearly indicates that the difference between the total moisture and deashing solvent level can be readily accounted for by the presence of water in the samples.

Due to the high water content of these samples, the removal of the deashing solvent could have been aided by the localized reduction in solvent partial pressure in the bed of solids. Demonstration of similar reductions in the deashing solvent levels in water free ash concentrate samples will clear up the ambiguity of the present test results.

Here are some general observations regarding the Nara test:

(1) Although the ash concentrate feed contained several hard chunks, 1-2 inches in diameter, the dryer operation was smooth. The dried product also contained agglomerates but they were much smaller than those in the feed.

(2) No problems, such as smoldering, were encountered during the course of the tests, indicating an effective nitrogen blanket over the material during the test.

(3) At the end of the tests, the top cover on the dryer was removed, the contents discharged, and the trough rinsed by a stream of water to allow inspection of the internals. A little bit of material was seen adhering to the vessel and paddle surfaces near the feed point. The fouling tendency decreased sharply with distance from the inlet—and beyond about 2 ft there was no visible evidence of adherence of material to the heat transfer surfaces.

FURTHER INVESTIGATION

Additional testing will be conducted at the S-B test center, which has now been upgraded to carry out the sort of drying tests mentioned above. The objectives of the proposed tests will be to:

(1) Determine the effect of purge nitrogen flowrates on residual solvent and fines carryover.

(2) Determine the effect of solids residence time and paddle speed on residual solvent level and particle attrition.

This information will be needed to design particulate removal, solvent recovery, and gas recycle systems to go with the Nara Paddle Dryer. If, after current mechanical modifications to the flash drum at Wilsonville the ash concentrate still has a high level of deashing solvent, then a Nara Paddle Dryer unit should be installed and its long term operability and optimum operating conditions determined.

The pilot unit model, NPD 1.6W, used in the present tests is ideally suited to handle the Wilsonville load.

Table 1

Laboratory Drying Tests of K-M Ash Concentrate in Nitrogen Atmosphere at 250, 300, and 350°F

Drying time (minutes)	Deashing solvent content of ash concentrate (wt %)		
	250°F	300°F	350°F
0	2.78	2.78	2.78
10	1.30	0.38	0.33
25	0.44	0.14	0.024
45	0.32	0.067	< 0.02
120	0.13	0.021	< 0.02
180	0.083	< 0.02	< 0.02
overnight[1]	< 0.02	< 0.02	< 0.02

1. Drying time was between 18 and 22 hours.

Figure 1

Nara Paddle Dryer

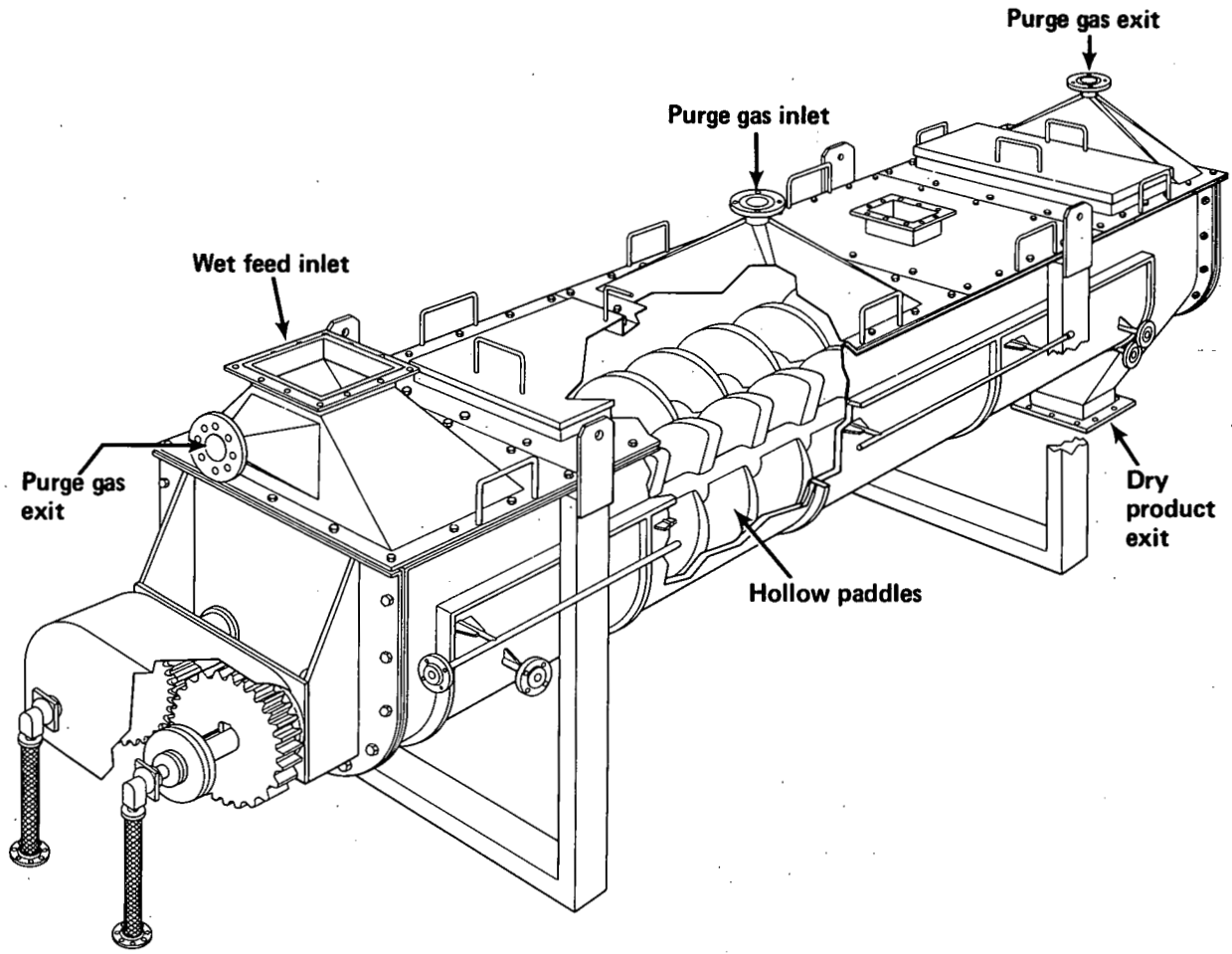

Figure 2

Flowsheet Of Nara Paddle Dryer

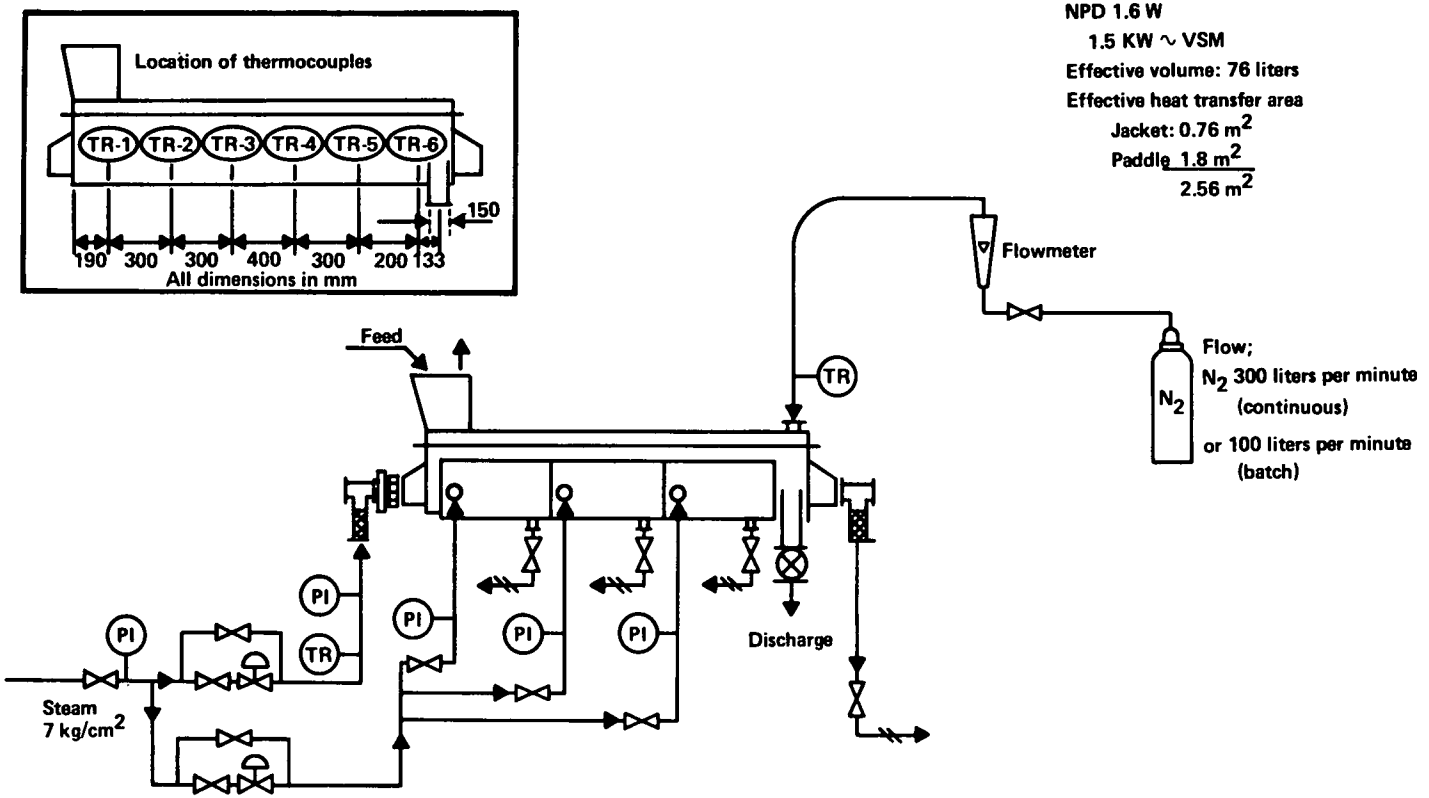

Figure 3

Drying Test of Kerr-McGee Ash

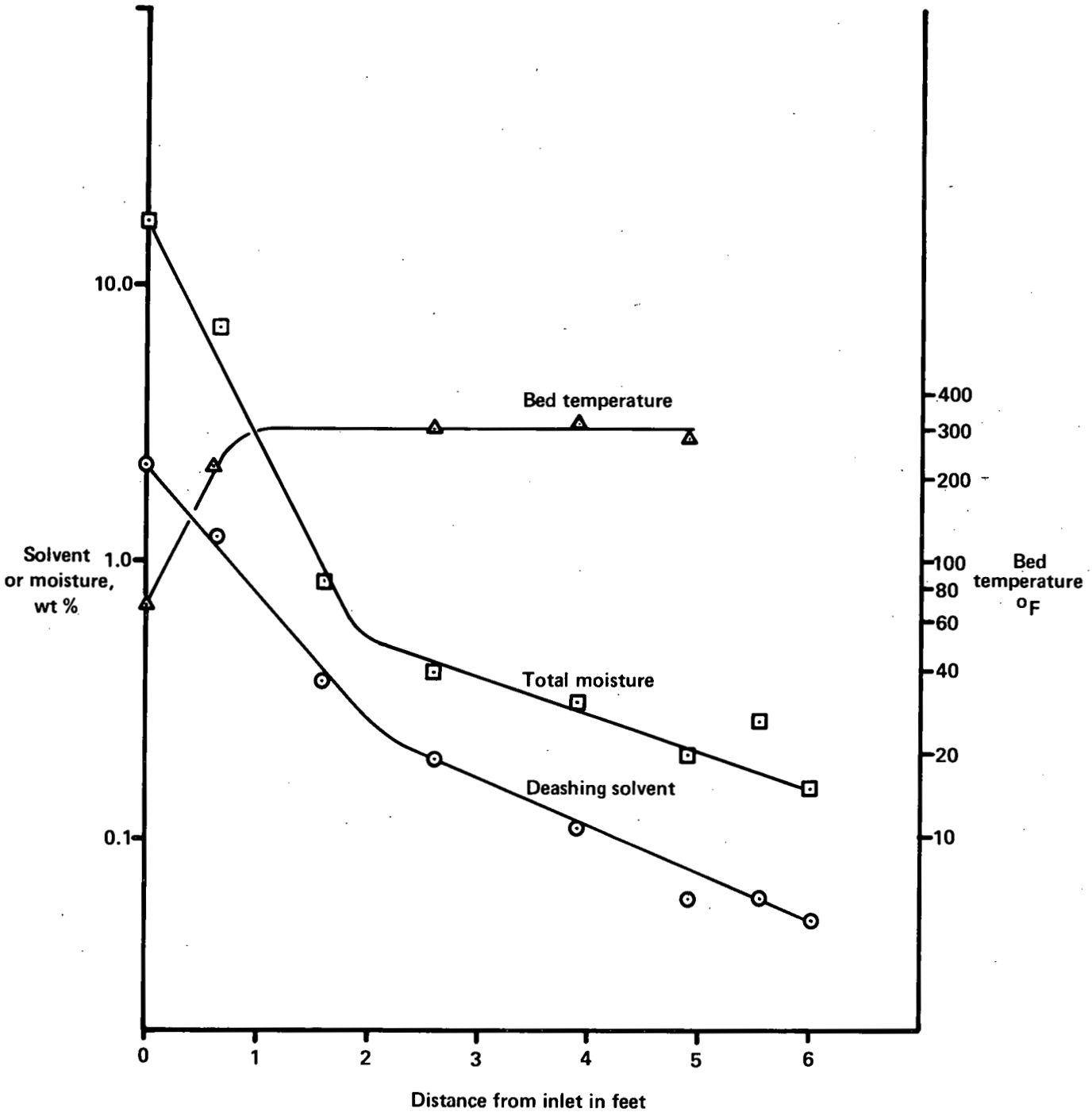

SLURRY FIRED HEATER UPDATE OF DATA BASE AND DESIGN OPTIONS

R. M. Thorogood*

The overall furnace heat duty calculated for the Phase 0 Demonstration Plant design has been confirmed recently by measurements of coal slurry enthalpy. These data also provide a basis for determining coal slurry enthalpy as a function of the temperature through the Slurry Fired Heater.

Other studies involving the Slurry Fired Heater include an investigation of the limiting heat fluxes that are permissible for various heat transfer modes and furnace configurations. A method has also been determined for assessing thermal stress limitations on heat flux.

An analysis of pressure drop data from the preheater in the Wilsonville Pilot Plant has been used to predict pressure drops in the gas-slurry flow system of the Demonstration Plant.

Further development of pressure drop and heat transfer data is one objective of the SRC-I experiments scheduled for May and June 1980 at Fort Lewis; they are described at the end of this article.

Alternatives to the all-convective design for the Slurry Fired Heater recommended in the Phase 0 Report are being explored and evaluated by Catalytic, Inc., the contractor for Area 12 of the Demonstration Plant, and by specialists in furnace design. This article discusses some of the factors under consideration.

* * *

This article covers the following topics:

- Coal Slurry Enthalpy Data
- Determining the Heat Flux to Fired Heater Tubes
- Analysis of Pressure Drop Data From the Wilsonville Preheater
- Fired Heater Design Options
- The SRC-I Experiments at Fort Lewis

* * *

*With L. R. Barrus, J. R. Freeman, and G. M. Wilson on enthalpy; B. O. Brown on heat flux; S. I. Clarke on pressure drop; and T. Thew on the Fort Lewis Tests. Thorogood, Brown, and Thew are from ICRC. Clarke is from Air Products and Chemicals, Inc. Barrus, Freeman, and Wilson are from Wilco Research Company.

COAL SLURRY ENTHALPY DATA

The results of six temperature-enthalpy runs on hydrogen-coal slurries show an average heat capacity between 230°F (110°C) and 775°F (412.8°C) of 0.57 Btu/lb-°F (0.57 cal/g-°C) with what appears to be a random scatter of ±5%. The results also indicate the following two-step coal conversion process in the region from 554°F (290°C) to 716°F (380°C):

(1) Solvation of the coal either by swelling or by actually going into solution (endothermic).

(2) Further chemical reaction of the solvated coal either by rearrangement or hydrogenation (exothermic).

The net effect of this two-step behavior is smaller at low heating rates than at faster heating rates. At average heating rates of 10.0°F/min (5.6°C/min) between 500°F (260°C) and 750°F (398.9°C), the effect is rather small, but at heating rates of 31.3°F/min (17.4°C/min) it becomes more significant. The effect at actual process conditions will be even more significant, because the anticipated heating rate will be about 41.4°F/min (23°C/min) for the same interval. The data from these runs give an initial basis for estimating the effect in the actual process.

Importance of Enthalpy

The enthalpy of hydrogen-coal slurries as a function of temperature is important because it relates to the amount of heat and heat exchanger surface area necessary to heat these streams to reaction temperature. The problem is complicated by the fact that conversion of the coal occurs during the heating stage of the process, so the temperature-enthalpy behavior is also dependent on the heating rate.

The main variables affecting enthalpy are temperature and heating rate. But other factors, such as the ratio of coal to solvent, the ratio of gas phase to slurry phase, and the agitation rate, could also affect the measured enthalpy data due to mass transfer and heat transfer effects.

This project, carried out at Wilco Research Company, Provo, UT, obtained temperature-enthalpy data on hydrogen-coal slurries composed of 200 mesh Kentucky #9 coal and Wilsonville process solvent. The effects studied this time were heating rate and the ratio of gas phase to slurry phase. Other effects—coal/solvent ratio, agitation rate, coal properties, and solvent properties—will be studied later.

Results of the Six Runs

The physical properties of the Wilsonville solvent and the Kentucky #9 coal used in the six temperature-enthalpy runs are detailed in Tables 1 and 2. Each run was measured at a constant weight ratio of coal to solvent of 0.61, except for one run made on a coal-free basis.

Heating rates for the temperature interval between 500°F and 750°F (260°C and 389.9°C) varied from 8 to 25 minutes, and the gas-to-slurry-volume ratio at room temperature varied from 0.46 to 0.58. At high temperatures the gas-to-slurry-volume ratio decreased due to the expansion of the slurry phase, so small differences at low temperature

became significant differences at higher temperatures. The ratios at the higher temperatures are not known because the densities at higher temperatures are not accurately known.

The run results are given in Figures 1, 2, and 3. Details of the runs follow:

Run number	Charge		Heating rate	
	Cell charge	Gas/slurry ratio (volume)	Rate	Minutes 250°C to 398°C
1	full	.47	slow	24.9
2	full	.47	fast	9.4
3	full	.47*	fast	8.6
4	reduced	.55	fast	8.0
5	reduced	.55	slow	20.7
6	reduced	.55	intermediate	14.1

*Gas/solvent ratio—no coal present.

Data on the H_2-slurry runs are plotted in Figure 1, where the curves have been shifted to an arbitrary enthalpy basis in order to separate them. The interval between 95°F (35°C) and 230°F (110°C) is a transient interval where a steady-state temperature is established between the cell and the heaters. The temperature-enthalpy data of interest appear above 230°F (110°C).

All of these curves show deviations from a smooth curve in the region of 572°F (300°C), corresponding to an initial endothermic region (deviation above the smooth curve) followed by an exothermic region (deviation below the smooth curve). This behavior relates to the two-step conversion process mentioned above: solvation (endothermic) and further chemical reaction (exothermic).

When the H_2-slurry mixture is heated slowly, the time lag between the two steps appears to have a smaller effect on the deviation curve than at higher heating rates. Thus Runs 1 and 5, which were heated slowly, show smaller deviations than do Runs 2 and 4, which were heated more rapidly. Run 6, which was heated at an intermediate heating rate, shows an intermediate deviation curve. If the deviation curves in Figure 1 are related to the solvation and other conversion reactions, then it would appear from Figure 1 that most of the conversion occurs in the region from about 554°F (290°C) to 716°F (380°C), depending on the heating rate. At low heating rates, the conversion appears to be completed at lower temperatures than at high heating rates—as would be expected.

Other effects that might explain the deviation curves in Figure 1—incomplete mixing in the cell causing hot spots or a leak from the cell—can be ruled out by examining Figure 2, a plot of pressure versus the percent of time interval between the initial and final temperature. Temperature errors associated with hot spots should be smoothed out in this type of plot because the pressure represents an average result of all temperatures in the cell.

Figure 2 shows a change in the slope of the pressure curves at about 67% of the run-time-intervals, corresponding to about 572°F (300°C). This coincides with the onset of the deviation in the curves in Figure 1—so the effect could not be explained by hot spots in the cell due to incomplete mixing; the same phenomenon that produces the deviations in the temperature-enthalpy curves of Figure 1 also produces the slope transitions in the pres-

sure curves of Figure 2. Nor would a leak explain the effect, because a leak would cause cooling and require additional heat to compensate, but the actual curve exhibits an exothermic region.

The solvation-conversion steps seem to be the explanation of the curves in Figure 1—a conclusion supported by the fact that the H_2-solvent run without coal (Figure 3) does not exhibit a deviation curve.

The overall effects of heating rate and cell charge on the enthalpy difference between 230°F (110°C) and 775°F (412.8°C) appear to be small. The average heat capacity of the cell charge between 230°F (110°C) and 775°F (412.8°C) is about 0.57 Btu/lb-°F (0.57 cal/g-°C), with an average deviation of ±5%, which appears to be the level of accuracy in these measurements.

Procedure and Apparatus

The temperature-enthalpy measurements were made in a nominal 950cc calorimeter assembly (shown schematically in Figure 4), which features these capabilities:

(1) Rapid heating from room temperature to 775°F (413°C)
(2) Pressures to 3000 psia
(3) Operable with H_2-coal slurries
(4) Low heat-leak

The basic apparatus is a 1000cc stainless steel cell containing a heater, thermocouple well, and connections for charging hydrogen and for pressure measurement. Coal and solvent are charged to the cell by opening one end. The end is replaced and sealed with teflon tape seal (teflon appears to seal adequately so long as the cell is not cooled after heating). The cell is then evacuated, pressurized with hydrogen from a metering pump, and installed in the apparatus for the temperature-enthalpy run.

During each run the cell is surrounded by a heat shield heated to the same temperature as the cell. The space between the cell and the heat shield is taken up by magnesium silicate insulation. Since both sides of the insulation are heated at the same rate, approximately half the insulation belongs to the cell and half belongs to the shield.

Pressure measurement in the cell is achieved by installing a small, stainless steel, 15 micron filter at the end of the line in order to avoid plugging of the line by hardened slurry. The cell and shield are heated with alternating current power, the amount of power being determined by measuring the voltage across the heater and across a standard 0.1 ohm resistor with an alternating current digital voltmeter.

Our maximum heating rates correspond to a power input to the cell of about 1000 watts. With a heater surface area of about 0.65 ft^2, this represents a heat flux of about 5000 Btu/hr-ft^2. With this heat flux, temperature gradients on the order of about 45°F could have existed between the heater and the rocked H_2-slurry mixture. A gradient of this magnitude is probably not serious insofar as interpreting the data is concerned, but a larger gradient would not be wanted. With this amount of power to the cell, it is necessary to heat the shield with about 3000 watts.

Two runs are made for each enthalpy run reported. The first is made with water in the cell; from this enthalpy of the calorimeter is determined, since the enthalpy of water is given in the American Society of Mechanical Engineers (ASME) steam tables. The second run is then made with the H_2-slurry mixture; from this the enthalpy of the H_2-slurry mixture is computed by subtracting the enthalpy of the calorimeter.

Calibration runs are made with each run because it is necessary to cut the calorimeter cell open to remove the contents of the previous run and then to reweld it shut (as shown by the weld bead in Figure 4). Since this operation changes the characteristics of the cell, a calibration is made each time.

* * *

DETERMINING THE HEAT FLUX TO FIRED HEATER TUBES

Two factors may limit the permissible heat flux to the process tubes in the Slurry Fired Heater: (1) the coal slurry film temperatures above which coke formation may occur; and (2) the maximum stress on the inside surface of the tube resulting from pressure and thermal differentials in the tube wall.

The former effect has been examined in a single-side fired radiant furnace and a convective furnace. The result shows that a higher overall heat flux is achievable for the radiant design because of the ability to vary the firing rate throughout the furnace, even with the high ratio of peak to average heat flux which occurs in a single-side fired furnace.

A method has been determined for the formation of thermal stress limitations on heat flux with the assistance of a consultant, H. C. Hottel, professor emeritus, Department of Chemical Engineering, Massachusetts Institute of Technology.

Heat Flux Variations and Temperature Limitations

Tubular heater designs are generally based on the calculation of an average heat flux. In reality, heat flux varies considerably with the location inside a heater. This occurs both axially and circumferentially around a tube. The latter causes a temperature variation around the tube cross section. The magnitude of the variation can be important if the process fluid is sensitive to temperature.

The extent of flux variations depends upon whether the tubular heater is convective or radiant.

Convective. For a cylinder in a flowing gas stream, the heat transfer coefficient, h, varies around the tube circumference as flow changes occur:

- Formation of laminar boundary layer
- Growth of laminar boundary layer
- Transition from laminar to turbulent boundary layer
- Growth of turbulent boundary layer
- Breakaway of boundary layer from tube surface

The extent of this variation is affected by:

- Reynolds number
- Tube position in bundle
- Lateral and transverse spacing of bundle
- Bundle layout (triangular or rectangular pitch)

Radiant. In a radiant furnace, variation in heat flux is caused by the changes in the view factor around the tube cross section. Such variations are affected by:

- Tube position within the furnace

- Ratio of the center to center spacing to tube diameter
- Location of heat source

Reference 1 in the bibliography following this section discusses the flux distribution around tubes in different types of radiant furnaces.

Since coking of the coal slurry is probable at film temperatures approaching 950°F, a study is being made to compare convective and radiant furnaces. It is not yet complete in that it does not include the effect of gas radiation in the convective furnace or in a doublefired radiant furnace arrangement.

Method of Analysis. A computer program has been developed which calculates the temperature distribution in a thick-walled tube for a given distribution of inside and outside heat transfer coefficients—and for specified tube diameter, wall thickness, and material properties. Thus, for given inside heat transfer coefficients, the maximum and average external heat flux corresponding to a maximum inside film temperature may be determined.

Procedures. A maximum film temperature of 950°F was selected as the limit for determining maximum heat flux. An 8-inch diameter, Schedule 160 furnace tube of 316 stainless steel (SS) was assumed. And these procedures were followed:

Convective. From Reynolds numbers obtained from typical convective design proposals together with tube layout, a curve relating the variation of the local outside transfer coefficient (H_O) to the average value was obtained from Reference 2. An average value for H_O was selected and assumed to be constant throughout the heater.

Inside local film temperatures were then calculated on the assumption of two-dimensional heat flow. Variations in the average value of the outside coefficient were taken until a value was obtained whereby the maximum local film temperature in any part of the heater just approaches 950°F. This value was then used to calculate the corresponding film temperatures in the other segments.

Radiant. A radiant furnace with the refractory walls lined with one row of tubes was considered in this study. It was assumed that the maximum heat flux could be changed in different parts of the heater. The path taken for the calculation of the inside film temperatures was exactly the same as for the convective design—except that heat flux instead of heat transfer coefficient was varied on the tube circumference.

Convective and Radiant Compared. Due to uncertainties for heat transfer in a three-phase system and the variation of slurry viscosity with temperature, the inside heat transfer coefficient (H_i) cannot be accurately calculated. Values between 20-35 Btu/hr-ft^2-°F may exist at slurry temperatures up to 550°F and this may increase to around 90-130 Btu/hr-ft^2-°F up to 750°F. The lowest values of these two ranges (20 and 90) were used as possible values for H_i, within the temperature ranges of 500-550 and 550-750°F, respectively.

Table 3 presents results obtained using the above values for H_i. An average value of 15.0 Btu/hr-ft^2-°F was found to be the highest allowable value for H_O. This was due to the occurrence of the maximum film temperature (950°F) within the lower range of the slurry temperature. However, if the assumed lower value for H_i was 35 Btu/hr-ft^2-°F, then it is possible to increase H_O to 18.0 Btu/hr-ft^2-°F. Here the maximum film temperature occurs in the higher temperature range of the slurry. Table 4 presents the latter results.

Results for the radiant furnace are shown in Table 5.

From a comparison of Table 3 with Tables 1 and 2, it is seen that the radiant design permits a higher average heat flux than the convective design. This happens in spite of the much higher peak-to-average heat flux ratio occurring in the radiant furnace. It is due to the fact that the radiant furnace will always be operating at the maximum permissible heat flux in all segments; in the convective design, this occurs in only one segment.

Summing Up. A computer program that calculates the temperature profile in a thick-walled tube for a specified geometry and tube material has evaluated maximum and average circumferential heat fluxes at various axial locations in a convective and a single-side fired radiant furnace. The radiant furnace required less surface than the convective furnace.

Thermal Stress Limitations of Heat Flux

The tangential stress in a heated thick-wall tube is made up of the pressure stress and a thermal stress that results from the temperature gradient through the tube wall. For heat flow into the tube the maximum stress occurs at the inside surface. Professor Hottel has recommended a procedure for calculating the tangential stress and his procedure has been used to examine the relationship between tube diameter, wall thickness, heat flux, and tangential stress for a 316 SS tube material.

The results indicate that for a heat flux of 10,000 Btu/hr-ft^2-°F, the stress in a 6-inch diameter Schedule 160 tube is approximately 18,000 psi compared to 21,000 psi for an 8-inch diameter tube. Minimum stress occurs in tubes of approximately Schedule 140, thicker tubes having a higher stress value.

These predictions will be compared with the procedure of the American Petroleum Institute (API) Recommended Practice 530, Calculation of Heater Tube Thickness in Petroleum Refineries. Thermal stress considerations may be significant in limiting the permissible heat flow in the Slurry Fired Heater.

References

(1) R. S. Fairall and L. A. Mekler, "Evaluation of Radiation Heat Absorption Rates in Tubular Heater." *Petroleum Refiner*, (June 1952).

(2) K. F. Martsinanskas, R. V. Ulinskas, and A. A. Zhukanskas, "Influence of the Geometry of the Tube Bundle on the Local Heat Transfer Rate in the Critical Region of Stream Line Flow." *Int. Chem. Eng.*, Vol. 7 (8), (1977).

(3) W. H. McAdams, *Heat Transmission*, 3rd edition. McGraw-Hill, New York.

★ ★ ★

ANALYSIS OF PRESSURE DROP DATA FROM THE WILSONVILLE PREHEATER

Pressure drop data from the Wilsonville preheater were compared to values predicted by various two-phase (gas/liquid) flow correlations. By matching observed and predicted pressure drops it was possible to back-calculate the apparent liquid viscosity, i.e., the slurry viscosity, at various temperatures within the preheater. Information obtained was used to predict pressure drop from the Demonstration Plant preheater.

Non-Newtonian Slurry Behavior at Wilsonville

The Wilsonville preheater data were interpreted to show a high slurry viscosity somewhere in the range of 400 to 600°F. There was significant evidence of non-Newtonian slurry

behavior, especially in the high viscosity region. To eliminate a wide spread in slurry viscosity predictions the two-phase pressure drop correlation required some modification to include the observed non-Newtonian behavior.

Four two-phase pressure drop correlations were evaluated for slurry viscosity calculations:

- Lockhart-Martinelli
- Dukler No-Slip
- Dukler Constant-Slip
- Chenoweth-Martin

The Chenoweth-Martin correlation was unsuitable, due to its range of applicability. The least spread in viscosity predictions occurred for the Dukler No-Slip model, where two-phase flow was assumed to behave as a homogenous mixture of average physical properties. Both Dukler models have an interesting characteristic built into them: with high viscosity liquids it is possible for increased gas flow rate to reduce pressure drop.

However, the data available for analysis was insufficient to develop a full understanding of coal/solvent/gas behavior. Many additional analyses will be required to determine such effects as:

- Type of coal
- Pipe diameter
- Non-Newtonian behavior
- Slurry viscosity vs temperature

Such analyses call for better pressure drop profiles than those currently available for the Wilsonville preheater.

Wilsonville Test Cases

Test cases E, I, K, N, P, R, U and W from Run 133 (Indiana V coal) were selected for analysis because a wide range of coal/solvent/gas flowrates would thereby be covered. Information on Run 133 was obtained from the Wilsonville Quarterly Report of January-March 1979. A brief summary of the test cases analyzed is shown in Table 6.

Preheater Measurements. For each test case, temperature (bulk fluid and skin) and pressure were reported for various positions within the preheater:

(1) Temperature. A plot of the skin-fluid temperature differences compared with the fluid temperature is presented in Figure 5 (which connects points for W, I, and R test cases, representing high, middle, and low gas-and-liquid flow rates). Figure 5 indicates a sharp increase in the skin-fluid temperature difference between 350 ft and 450 ft into the preheater. This suggests that an endothermic reaction occurs between 450-600°F, probably due to solvation of coal particles—a matter of interest because dissolving the coal particles may swell with the adsorption of solvent and form a gel-like slurry of high viscosity.

(2) Pressure Drop. Unfortunately, pressure tappings are less numerous than thermocouples in the Wilsonville preheater. From Figure 5 it can be seen that the first pressure drop measurement is taken for over half of the total preheater length and includes the last 70 ft where gel formation might be significant. Reduced pressure gradients in subsequent sections of the preheater suggest a significant decrease in fluid viscosity once solvation of coal is completed.

Evaluating Pressure Drop Correlations

The four methods of correlating two-phase pressure drops may be summarized as follows:

Lockhart-Martinelli (Empirical). The most widely used and accepted correlation in industry. This is most certainly due to the ease with which calculations are made and the conservatively high predictions of pressure drop. Except for a few data points, the correlation was developed with low viscosity fluid (i.e., water) and small diameter pipes.

Dukler Constant-Slip Model. A semi-empirical/theoretical correlation which assumes that slip between gas and liquid takes place, but that the ratio of phase velocity to average homogenous velocity is constant across a cross section.

Dukler collected a data base of over 2,500 points and tested many two-phase pressure drop correlations against his own. He claimed that while the Lockhart-Martinelli correlation gave marginally better results for small diameter pipe and low viscosity fluids, his own constant-slip method proved best over the widest range of conditions (e.g., large pipe diameter, high liquid viscosities).

However, Dukler's method has not yet won general acceptance in industry. This is because of the complexity of calculations requiring determination of in-situ volumetric hold-up, and the fact that the pressure drop predictions are only marginally more accurate than those of Lockhart-Martinelli.

Dukler No-Slip Model (Theoretical). Assumes two-phase flow to be a homogenous mixture. Physical properties of the mixture are the mean of gas and liquid properties, the contribution of each phase determined by the volume fraction of its flow rate. Homogenous pressure drop must always be less than the actual two-phase pressure drop where additional losses occur from the interaction of the phases.

Chenoweth-Martin (Empirical). Not widely used. Its applicability is restricted by an upper limit for the ratio of liquid to gas viscosity. Early in the analysis of Wilsonville data it was realized that this limitation was too severe for SRC preheater fluids and the Chenoweth-Martin correlation was discarded.

Method of Calculating Slurry Viscosity

Physical properties and flowrates for each test case were derived as functions of temperature. Assumed values of slurry viscosity were then varied until the pressure gradient as calculated by the correlation matched the pressure gradient as measured. Flow conditions were related to position in the preheater by reference to the temperature profile.

No slurry viscosities were calculated for temperatures between 100-400°F. In this region, approximately the first 120 ft of the preheater, slurry viscosity was assumed to average 100 lb/ft-hr. Pressure drop for the initial 120 ft could thus be calculated and subtracted from measured pressure drop for the first 376.7 ft. A better estimate of pressure drop, and hence of liquid viscosity, could be made for the more important middle section of the preheater, where gel formation and high viscosities were suspected to occur. Viscosities so determined were 10% to 30% higher than those evaluated for the whole 376.7 ft when making no assumptions about inlet viscosity.

Gas viscosities were estimated to be in the range of 0.03 to 0.05 lb/ft-hr. The choice of gas viscosity within this range was found to have very little effect on the back-calculated values of slurry viscosity. Largest differences in slurry viscosity occurred for the Lockhart-

Martinelli correlation and these were in the order of 2% or less. Consequently, all results reported here were determined with gas viscosity set at 0.05 lb/ft-hr.

Results of Slurry Viscosity Determinations

Results are presented here for each two-phase pressure drop correlation with slurry viscosities for each pressure gradient plotted against position in the preheater. For a given pressure gradient, two viscosities were determined, both representing average values for that particular pressure gradient, but calculated by using flow conditions existing at the extreme ends of that section of the preheater. Approximate temperatures for these positions are also indicated.

Since the analysis was completed, it has been learned that Test E was taken immediately prior to an emergency blow at Wilsonville. All other tests were taken subsequent to this event. This may explain the discrepancy between Test E and the other points analyzed.

Pressure drops recorded for the last two sections of the preheater (i.e., approximately 600-800°F) were mostly very low, and probably beyond the level where worthwhile distinctions between individual test cases could be made. Table 1 will confirm this observation.

Slurry Viscosity Predictions by Lockhart-Martinelli Correlation. Figure 6 reports individual test case viscosities derived by the Lockhart-Martinelli correlation. A wide spread of liquid viscosities is observed between the eight test cases. Disregarding Test E, the plot shows that:

(a) As mean homogenous velocity (or gas flow rate) increases, slurry viscosity decreases for the 400-600°F preheater section.

(b) As temperature increases above 600°F, test cases with the highest total mass flow rates maintain relatively high slurry viscosities, while those with lower flow rates have significantly reduced viscosities.

Dukler Constant-Slip Model. Test case viscosities derived by the Dukler Constant-Slip correlation are summarized in Figure 7. They are very similar to those obtained in the Lockhart-Martinelli correlation with closest agreement occurring for flows of low gas content in the 400-600°F range—which is not surprising, since the two correlations agree with each other for single-phase flow. The pattern of viscosity versus flow rate is repeated.

Compared to Lockhart-Martinelli (see Figure 6), the Dukler Constant-Slip method has reduced the spread of viscosity values by 35% to 20%, the greatest improvement occurring in the 400-600°F section. Viscosities derived for the 750-800°F temperature range are all substantially higher than those of Lockhart-Martinelli.

Dukler No-Slip Model. Results for the Dukler No-Slip method are plotted in Figure 8. It is immediately apparent that the spread of viscosity predictions is markedly reduced; viscosities get progressively higher than those of the Dukler Constant-Slip method as flows approach the preheater outlet. A closer examination of the results shows a change in the relative order of test cases—the only exceptions to this being cases P and R, which are solvent feed only. Test case R, with the lower flow rate, shows consistently higher viscosities than test case P throughout the entire preheater.

The inlet section of the preheater, 400-600°F, now has test cases with low total mass flow rate tightly grouped around test case R. Those with a high total mass flow rate are tightly grouped around test case P. In the temperature range of 750-800°F, these two new groups develop: cases with high gas content which have high liquid viscosities; and those with little gas flow which have low liquid viscosities.

Chenoweth-Martin Correlation. This model produces marginally lower pressure drops for two-phase flow than does Lockhart-Martinelli for the same flow conditions and physical properties. Its range does not fully cover the low gas/liquid viscosity ratios experienced in the Wilsonville preheater. Therefore, a full analysis of this method was not performed.

Significant Difference Between Correlations

The Dukler Constant-Slip and Dukler No-Slip methods are significantly different from Lockhart-Martinelli in that the friction factor for two-phase flow is calculated from a Reynolds number based on a mean homogenous mixture viscosity, the contribution of each phase based on its flowing volume fraction. Due to high slurry viscosities, flow regime in the Dukler No-Slip and Dukler Constant-Slip methods was always laminar for the Wilsonville test cases. As such, the friction factor, f, was determined from $f = 16/Re$ and increases in gas content with solvent evaporation resulted in significantly lower values of f. As a consequence, lines drawn in Figures 7 and 8 slope upwards with increasing temperature, while those for Lockhart-Martinelli (Figure 6) slope downwards.

An interesting concept is thus seen to be built into the Dukler No-Slip and Dukler Constant-Slip methods. For sufficiently high liquid viscosities where homogenous flow is considered laminar, addition of gas can result in a reduction of pressure drop.

Overall test case viscosity determinations are seen to progressively increase in value when using the Lockhart-Martinelli, Dukler Constant-Slip and Dukler No-Slip methods respectively. Greatest differences occur in the outlet section of the preheater.

This is attributable to the increasing tendency of the models to use homogenous properties based on the flowing volume fraction of each phase. Increasing gas content with temperature results in viscosities and densities weighted more towards gas phase properties. Consequently, high liquid viscosities are required to obtain the required pressure gradient.

Two-Phase Flow Regimes

Horizontal flow regimes for the Wilsonville test cases and Demonstration Plant flow rates are depicted on the Baker flow graphs in Figures 9a and 9b. The Demonstration Plant preheater is shown to operate well into the bubble flow regime. Wilsonville test cases generally start off in the bubble regime, but slip over into slug flow on passage through the preheater.

All flow regime predictions assume an interfacial tension of 30 dynes/cm.

Evaluating Results

The small number of test cases and the questionable accuracy of pressure drop measurements in latter sections of the preheater make it unwise to form definitive conclusions concerning pressure drop behavior of gas/liquid/coal mixtures. More data with different coals and ranges of flowrate preheater dimensions and a more accurate pressure drop profile are required before this can be achieved.

The following discussion provides an indication of general trends to look for in slurry preheater pressure drop behavior . . . uses test case results for comparing the relative merits

of two-phase drop correlations . . . and looks for inadequacies that may exist in the two-phase gas/slurry approach to determining slurry preheater pressure drops.

Gel Formation. All four correlations showed slurry viscosity to peak between 400-600°F with values as high as 1600 lb/ft-hr. Figures 5 and 6 indicate that this coincides with the previously mentioned increase in skin fluid temperature difference—and provides supporting evidence of gel formation as coal dissolves into the solvent, a phenomenon also observed in other data sources.

Non-Newtonian Behavior. Two test cases, P and R, have no inlet feed gas and are essentially slurry flow. Vaporization of the solvent only increases the vapor content from zero at the inlet to about 10%, by volume, at the preheater outlet. Yet test case R, having the lower flow rate, is consistently seen to have a higher slurry viscosity throughout the preheater. This is an indication of Non-Newtonian Slurry Behavior.

The high viscosity region of Figure 6 shows a decrease of the apparent slurry viscosity as the gas fraction in the two-phase flow increases. This may be interpreted as a non-Newtonian behavior of the slurry in which the viscosity is reduced by the increased shear rate in the presence of gas.

An obvious improvement to the two-phase pressure correlation is the incorporation of non-Newtonian slurry behavior. It is planned to attempt this by modification of the liquid phase pressure term in the two-phase correlations.

* * *

FIRED HEATER DESIGN OPTIONS

The Phase 0 design specified to vendors in early 1979 was based upon two principal assumptions:

(a) Each furnace tube circuit would have its own slurry feed pump to prevent any possibility of flow maldistribution.

(b) To minimize circumferential heat flux variations, an all-convective design was preferred.

But two significant problems have resulted from these assumptions:

(a) It may be difficult to provide instantaneous backup with either solvent or slurry pumps in order to prevent flow loss and coking in the fired heater.

(b) It is very difficult to sight the inner pipe circuits of the convective tube bank for either maintenance or decoking.

To evaluate alternatives, radiant and convective layouts are currently being prepared by the SRC area subcontractor, Catalytic, Inc.

Various combinations of pumps, exchangers, and fired heaters are shown in Figures 10, 11, and 12. The factors being considered in evaluating these layouts are flow distribution control, flow backup in the event of pump failure, and operability and spare requirements.

Two variants that occur in the Slurry Fired Heater depend on the selection of the pipe diameter. The Phase 0 design used 9-inch diameter Schedule 160 pipe and required six parallel pipe circuits. The alternative of 6-inch diameter pipe allows a significant cost reduction for pipe material, but increases the number of parallel circuits to 10 or 12. To comply with the requirement of one pump to a circuit adds complexity into the pump and heat exchanger system. Both choices allow the use of two 50% duty heaters without major ad-

ditional cost when compared to a single 100% duty heater; two heaters are now a specified requirement for the Demonstration Plant design.

Radiant-convective furnace layouts are being studied with emphasis on these variables: process fluid film temperature and heat flux variation (coking potential); local heat flux variation with turndown; pipe stress; process flow regime; pressure drop; potential for erosion or solids accumulation.

The preferred layout will be optimized with respect to tube diameter, layout, and spacing. Calculations will be made of heat flux distribution, and tube wall temperature distribution to ensure that the maximum film temperature of the slurry does not exceed 900°F. These calculations will require correlation of heat transfer data from Fort Lewis, which are not expected to be available until this summer.

* * *

THE SRC-I EXPERIMENTS AT FORT LEWIS

Two major experimental programs have been proposed by ICRC to be run at Fort Lewis in support of the SRC-I Demonstration Plant design: the Slurry Fired Heater tests and High Temperature Slurry Mix tests. They are currently scheduled for May and June 1980.

The Fired Heater tests are a series of baseline runs followed by coal slurry runs. The baseline runs will provide reference pressure drop data and heat transfer information in the absence of coal. For a recycle solvent rate of 10,000 lb/hr, H_2 gas rates over the range of 50-500 lb/hr (mass flow of pure H_2) will be run in two modes, unheated and heated. The first set will determine flow stability at a known liquid viscosity under isothermal conditions (solvent temperature = 350°F). The second set replicates the flow specifications of the first set with the two-phase system heated to a targeted outlet temperature of 800°F.

The coal slurry runs will provide fundamental heat transfer and pressure drop data in support of the Demonstration Plant Fired Heater design. A matrix of experiments covering a range of coal slurry rates of 5000-11,000 lb/hr and H_2 gas rates of 50-500 lb/hr has been developed. Imbedded in the matrix are slurry/H_2 flow ratios that correspond to current Demonstration Plant design conditions.

The first set of experiments will examine the effect of H_2 gas rate at a fixed slurry rate of 10,900 lb/hr (essentially the maximum of the Fort Lewis plant). The second set repeats the first at 50% turndown conditions. A third set fixed the H_2 gas rate while varying the slurry rate from 5500 lb/hr to 11,000 lb/hr. In completing this matrix, duplication of earlier flow conditions will help to determine statistical variability and provide a clue to coking rates. Time has been provided for a fourth unspecified test which will be based upon interpretation of earlier results.

The High Temperature Slurry Mix tests will determine operating reliability of the Slurry Blend Tanks at elevated temperatures. The experiments are prompted by economic factors and favor recyle of hot process solvent, thereby eliminating the need for a preheat exchanger and/or reducing the duty of the Fired Heater. For a fixed slurry rate of 9100 lb/hr and H_2 gas rate of 81 lb/hr, the Slurry Blend Tank temperature range is targeted at 350-450°F. The yield structure will be monitored.

All slurry experiments will be using Kentucky 9&14 coal from the Colonial Mine. Although this coal differs from the Kentucky 9 coal designated for the Demonstration Plant,

it was selected for the tests because its reactivity is well-documented and it is relatively noncorrosive. Other general specifications include use of a full dissolver volume (92 ft^3) at 850°F and 2000 psi (if feasible). H_2 gas purity is set at 86% (by volume), which roughly corresponds to 50% by weight.

Careful monitoring of various parameters is being devised. In addition to the routine logging of flows, temperatures, and pressures pertinent to these tests, a high-speed recorder will identify flow regime transitions in the Fired Heater. For correlation purposes, solvent quality will be determined on a regular basis by a microautoclave apparatus recently obtained from Wilsonville. This solubility test is especially important to the proper conditioning of the raw solvent (anthracene oil) since such capabilities have not been present at Fort Lewis heretofore.

Prior to the test program on the Fired Heater a computer program is being assembled for rapid prediction and correlation of pressure drop, flow regime, and heat transfer using two-phase Newtonian flow models.

The specific correlations included for flow regimes are:

Baker—horizontal
Heat Transfer Research, Inc.—horizontal
Taitel-Dukler—horizontal and inclined

For pressure drop:

Lockhart-Martinelli

For heat transfer:

Collier-Lacy-Pulling
Chen

It is planned to run the program through a portable terminal for data assessment directly at Fort Lewis.

Table 1

Analysis of Wilsonville Process Solvent

Distillation cuts, °F	Wt %	Elemental analysis (wt %)			
		Carbon	Hydrogen	Nitrogen	Sulfur
IBP-420°F	1.34	84.81	9.90	0.40	0.19
420-550°F	53.92	87.45	9.34	0.44	0.30
550-850°F	32.57	88.38	8.54	1.08	0.30
850°F-FBP	12.16	86.64	7.35	1.59	0.67

Table 2

Analysis of Coal

	Kentucky #9[1] coal
Proximate analysis, wt %	
Moisture	1.82
Ash	10.08
Volatiles	37.86
Fixed carbon	49.35
Ultimate analysis, wt %	
Carbon	69.33
Hydrogen	4.66
Nitrogen	0.90
Sulfur	2.95
Sulfate S	0.04
Pyritic S	1.83
Sulfate ash, wt % (700°C)	13.45
Aluminum, wt %	1.53
Iron, wt %	1.45
Titanium, ppm	570
Boron, ppm	590
Chlorine, ppm	2400
Calcium, ppm	90
Magnesium, ppm	850
Potassium, ppm	2700
Sodium, ppm	470
Solvent solubilities, wt %	
Toluene	0
Pyridine	16.5[2]

1. Analytical results based on samples as received.
2. Includes 1.82% moisture.

Table 3

Calculated Film Temperature and Heat Flux

Convective furnace, H_O(avg): 15.0 Btu/hr-ft^2-°F

H_i, Btu/hr-ft^2-°F	T_{bulk}, °F	$T_{outside}$, °F	Q_{max}/Q_{avg}	Q_{avg}, Btu/hr-ft^2	$T_{film\ max}$, °F
20.0	500	1150	1.17	4810	809
20.0	530	1400	1.17	6440	943
20.0	540	1300	1.17	5630	901
20.0	550	1250	1.17	5180	882
90.0	530	1400	1.17	10150	678
90.0	570	1500	1.17	10860	728
90.0	625	1680	1.17	11380	791
90.0	750	1800	1.17	12260	979

H_i is the inside heat transfer coefficient.

H_O is the outside heat transfer coefficient.

T_{bulk} is the coal slurry temperature.

Q is heat flux.

$T_{outside}$ is the convective flue gas bulk temperature.

$T_{film\ max}$ is the maximum inside wall or slurry film temperature.

Table 4

Calculated Film Temperature and Heat Flux

Convective furnace, H_O(avg): 18.0 Btu/hr-ft^2-°F

H_i, Btu/hr-ft^2-°F	T_{inside}, °F	$T_{outside}$, °F	Q_{max}/Q_{avg}	Q_{avg} Btu/hr-ft^2	$T_{film\ max}$, °F
35	500	1150	1.17	6710	748
35	530	1400	1.17	8990	862
35	540	1300	1.17	7850	830
35	550	1250	1.17	7230	817
90	530	1400	1.17	11660	700
90	570	1500	1.17	12460	752
90	625	1600	1.17	13070	816
90	750	1800	1.17	14070	956

H_i is the inside heat transfer coefficient.

H_O is the outside heat transfer coefficient.

T_{bulk} is the coal slurry temperature.

Q is heat flux.

$T_{outside}$ is the convective flue gas bulk temperature.

$T_{film\ max}$ is the maximum inside wall or slurry film temperature.

Table 5

Maximum and Average Heat Fluxes for Radiant Furnace

H_i, Btu/hr-ft^2-°F	T_{bulk}	Q_{max}, Btu/hr-ft^2	Q_{avg}, Btu/hr-ft^2	Q_{max}/Q_{avg}
20	500	8490	5780	1.47
20	525	7960	5410	1.47
20	550	7420	5050	1.47
35	500	14450	9520	1.52
35	525	13420	8840	1.52
35	550	12730	8390	1.52
90	525	32720	20450	1.60
90	600	27470	17500	1.57
90	675	21660	13540	1.60
90	750	16130	10080	1.60

$T_{film\ max}$ — the maximum inside wall or slurry film temperature — is constant at 950°F.
H_i is the inside heat transfer coefficient.
T_{bulk} is the coal slurry temperature.
Q is heat flux.

Table 6

Summary of Wilsonville Test Cases

Page 1 of 2

Test	Date	Time	Slurry % MF	Coal MF lb/hr	B102 Slurry Preheater Inlet, psig	Feed gas, scfh	Bypass, scfh	Outlet, °F	Mix, °F	Conv, % MAF	SRC, % MAF	Sulfur in SRC, wt %	R101 Dissolver Inlet, °F	Outlet, °F	Conv, % MAF	SRC, % MAF	Sulfur in SRC, wt %
A	6 Jan	2400	37.9	406	2,450	9,230	0	765	748	58.6	19.4	1.43	745	855	95.9	21.5	0.60
B	7 Jan	0500	37.7	388	2,450	7,900	1,900	791	732	59.4	23.2	1.62	733	814	94.3	23.7	0.76
C	7 Jan	0920	36.7	402	2,450	8,300	1,970	790	730	75.6	26.9	1.54	735	825	94.7	22.7	0.77
D	7 Jan	1615	37.4	444	2,445	8,800	2,120	782	722	71.0	25.1	1.52	728	843	94.6	26.4	0.68
E	7 Jan	2030	37.4	444	2,430	5,280	5,090	826	711	89.0	27.5	1.65	717	780	93.4	30.4	0.99
F*	11 Jan	0100	38.7	387	2,450	4,520	1,190	775	725	-	-	-	724	850	95.2	21.1	0.61
	16 Jan	1845	36.7	446	2,450	4,090	970	795	730	74.9	29.4	1.86	733	840	95.6	24.9	1.0
G	17 Jan	0300	37.5	434	2,450	3,010	2,010	823	738	88.9	22.7	1.99	745	843	95.1	20.9	0.60
H	17 Jan	1000	37.8	435	2,450	2,320	2,710	832	739	90.3	19.1	1.45	748	847	95.3	21.3	
I	18 Jan	0215	36.8	440	2,450	4,900	3,890	856	742	91.9	30.9	1.27	751	841	95.3	20.8	0.60
J	18 Jan	1700	37.9	450	2,430	2,920	4,160	853	739	91.2	17.9	-	748	843	95.2	21.1	0.70
K	20 Jan	0120	38.4	598	2,470	10,116	0	762	742	52.7	22.4	1.58	747	845	94.6	28.2	0.69
L	20 Jan	1045	38.1	609	2,460	4,413	4,438	850	748	91.3	32.1	1.52	757	844	94.7	21.6	0.64
M	20 Jan	2106	37.6	610	2,430	0	3,431	851	755	92.6	26.5	1.44	759	846	94.0	25.5	0.83
N	21 Jan	1100	39.4	824	2,500	10,198	0	766	745	60.8	22.3	1.73	750	838	94.7	25.3	0.85
O	21 Jan	1725	38.9	722	2,450	5,524	4,145	850	752	92.4	32.9	1.57	760	847	94.4	23.7	0.70
P	22 Jan	0305	37.8	832	2,425	0	4,447	848	757	89.2	25.6	1.34	767	848	96.0	28.5	0.90
Q	22 Jan	1940	38.4	297	2,450	1,136	2,388	851	732	93.9	21.4	1.38	728	841	96.6	17.1	0.57
R	23 Jan	2128	37.4	323	2,430	0	1,821	850	738	93.4	29.3	1.35	736	844	95.1	18.6	0.65
S	24 Jan	0500	38.2	573	2,440	0	2,608	849	745	91.7	29.8	1.30	747	852	97.5	20.6	0.64
T	24 Jan	2040	37.9	779	2,490	9,746	0	763	734	64.8	21.6	1.59	751	845	95.3	22.8	0.63
U	25 Jan	1323	36.7	401	1,760	2,581	3,743	847	717	90.7	31.8	1.60	736	848	94.8	21.9	0.61
V	26 Jan	1700	36.7	291	1,760	5,097	2,143	847	762	90.6	25.0	1.24	762	850	95.7	17.9	0.63
W	27 Jan	0545	35.2	821	1,850	9,060	0	778	765	68.3	23.6	1.64	770	842	94.1	27.8	0.86
X	27 Jan	1115	37.9	640	1,710	0	3,300	849	759	90.2	28.1	1.93	763	845	93.9	26.3	0.86
Y	28 Jan	0450	38.9	336	1,750	0	1,884	850	750	91.7	28.8	1.54	748	834	93.8	22.5	1.08
Z	28 Jan	1605	25.8	357	1,750	0	2,003	848	776	90.3	19.3	1.42	778	832	94.6	15.1	0.84
A-A	29 Jan	1330	24.8	608	1,780	0	2,500	848	794	87.8	19.1	1.52	802	847	94.1	21.9	0.91
B-B	30 Jan	0930	36.2	422	2,475	9,480	0	766	741	52.2	25.9	1.78	816	847	95.7	22.2	0.61

*R101 Dissolver blowdown due to emergency shutdown; high pressure sample not taken; 352 lb solids containing 77% ash removed; 199 lb added to R101 to start.

Table 6

Summary of Wilsonville Test Cases

Page 2 of 2

Run	Slurry flow rate, lb/hr	Gas flow rate, lb/hr	Pressure drop, psia				Gas flow rate, scf/ton MF coal
			Total	Section			
				Inlet	Middle	Outlet	
A	1071	9230	60	36	14	10	45470
B	1029	7900	60	39	14	7	40720
C	1095	8300	58	37	14	7	41300
D	1187	8800	57	34	16	7	39640
E*	1187	5280	51	39	9	3	23784
F	1215	4090	74	53	16	5	18347
G	1157	3010	75	63	9	3	13871
H	1151	2320	75	61	11	3	10667
I*	1196	4900	75	64	8	3	22273
J	1187	2920	68	61	4	3	13000
K	1557	10116	105	74	15	16	33833
L	1598	4413	84	68	12	4	14500
M	1622	0	70	61	5	4	0
N*	2091	10198	110	68	24	18	24750
O	1856	5524	84	71	10	3	15302
P*	2201	0	77	65	8	4	0
Q	773	1136	53	45	5	3	7650
R*	864	0	51	45	4	2	0
S	1500	0	59	51	5	3	0
T	2055	9746	107	63	27	17	25000
U*	1093	2581	65	57	5	3	12873
V	793	5097	63	56	4	3	35031
W*	2332	9060	113	69	26	18	22070
X	1689	0	59	50	5	4	0

Asterisked test labels are data points that are analyzed in the text.

Figure 1
Enthalpy vs. Temperature
Comparison of H_2 - Slurry Runs
(Curves Shifted to Arbitrary Basis)

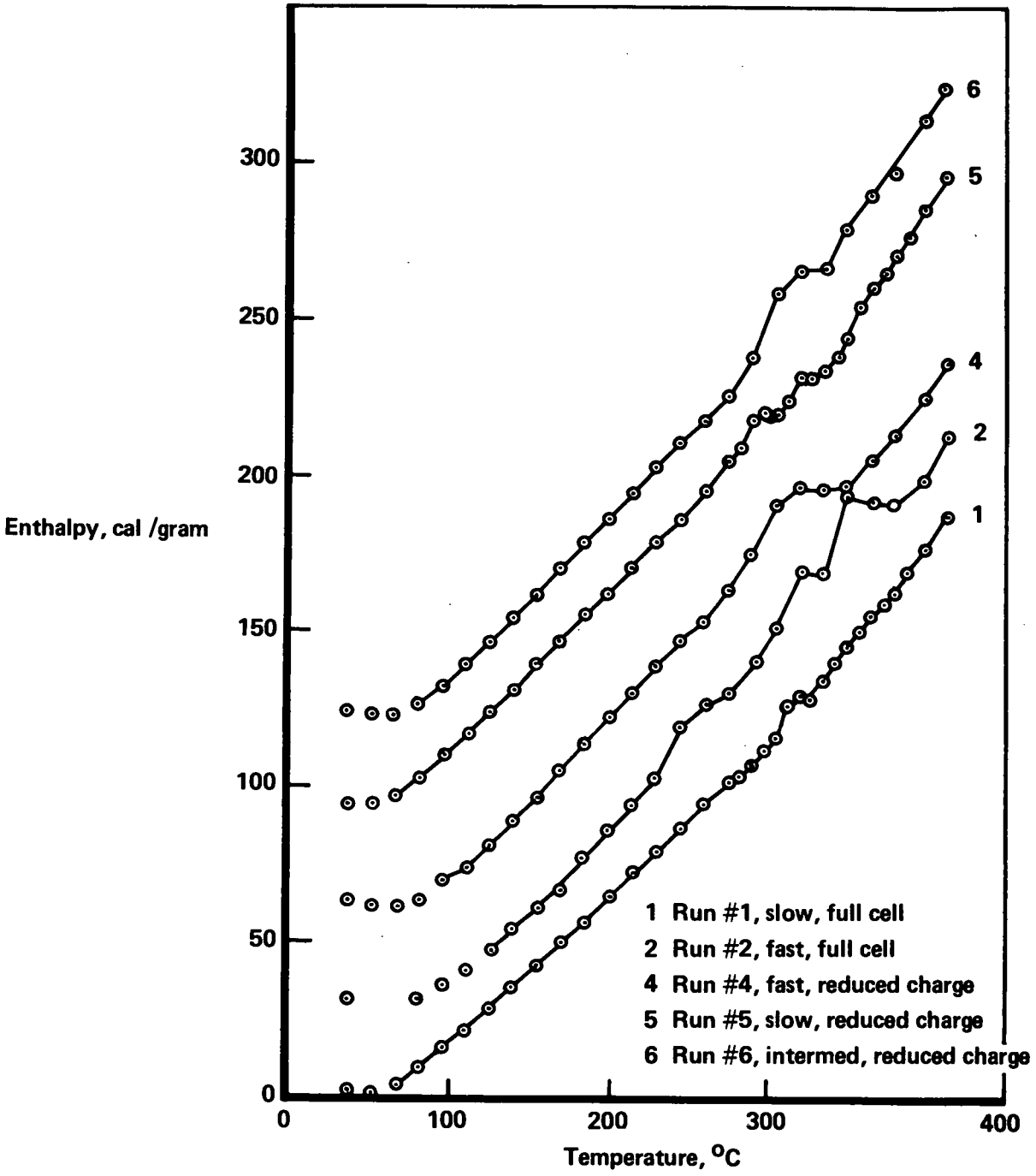

Figure 2

Pressure vs Percent of Run-Time-Interval, Comparison of All Six Runs

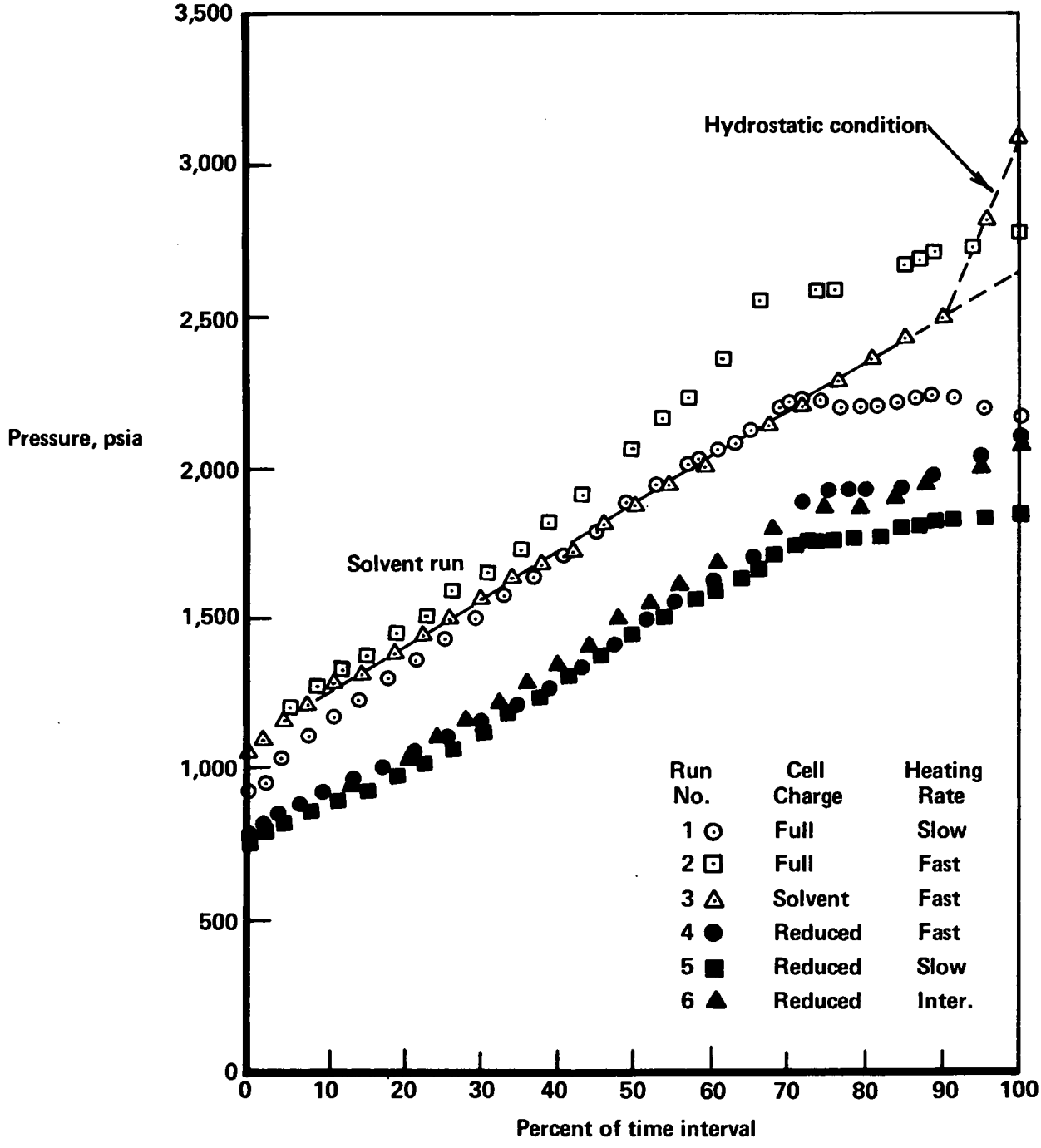

Figure 3
Enthalpy vs. Temperature Without Coal
Run #3

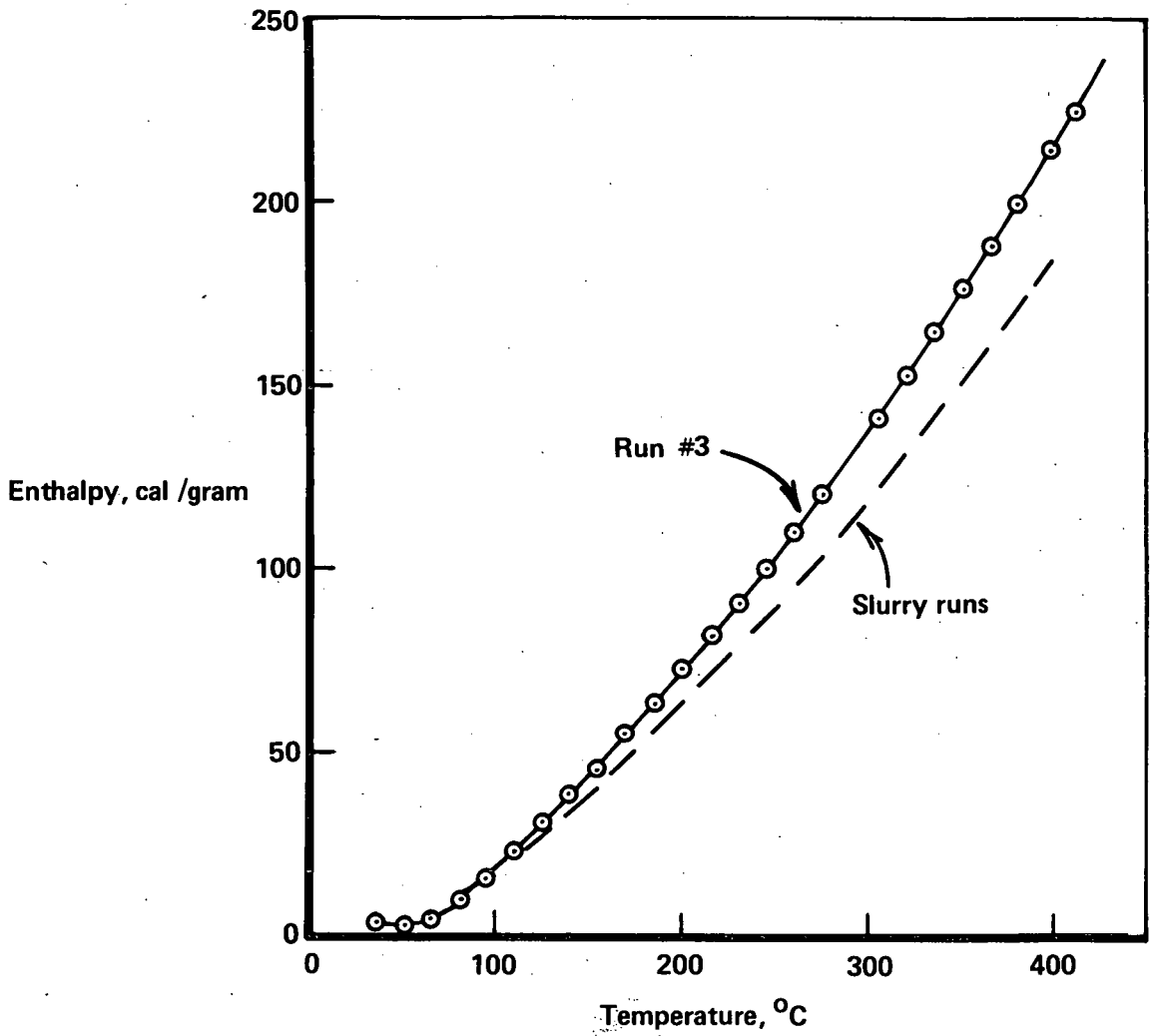

Figure 4
Schematic of Rocked Calorimeter Assembly for H_2-Slurry Temperature-Enthalpy Measurements

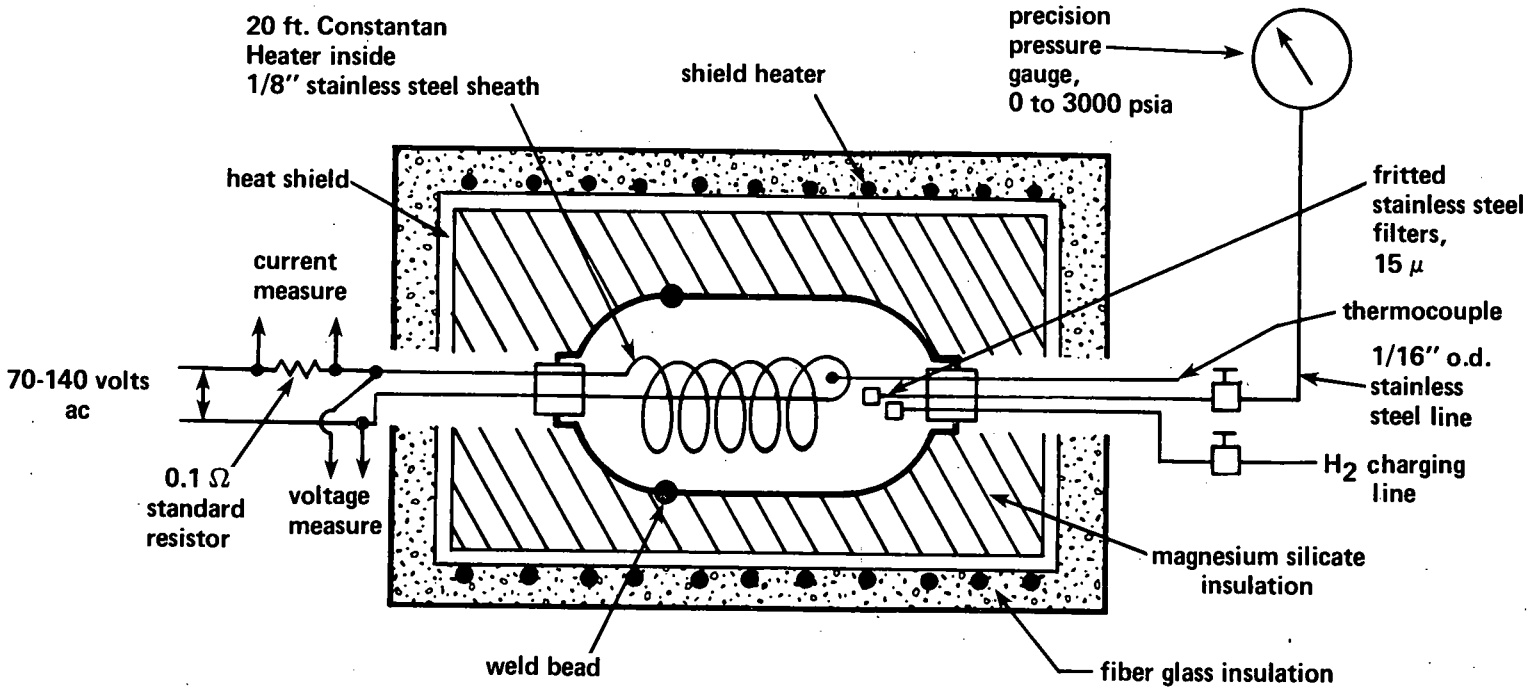

Figure 5

Skin-Fluid Temperature Difference vs. Fluid Temperature

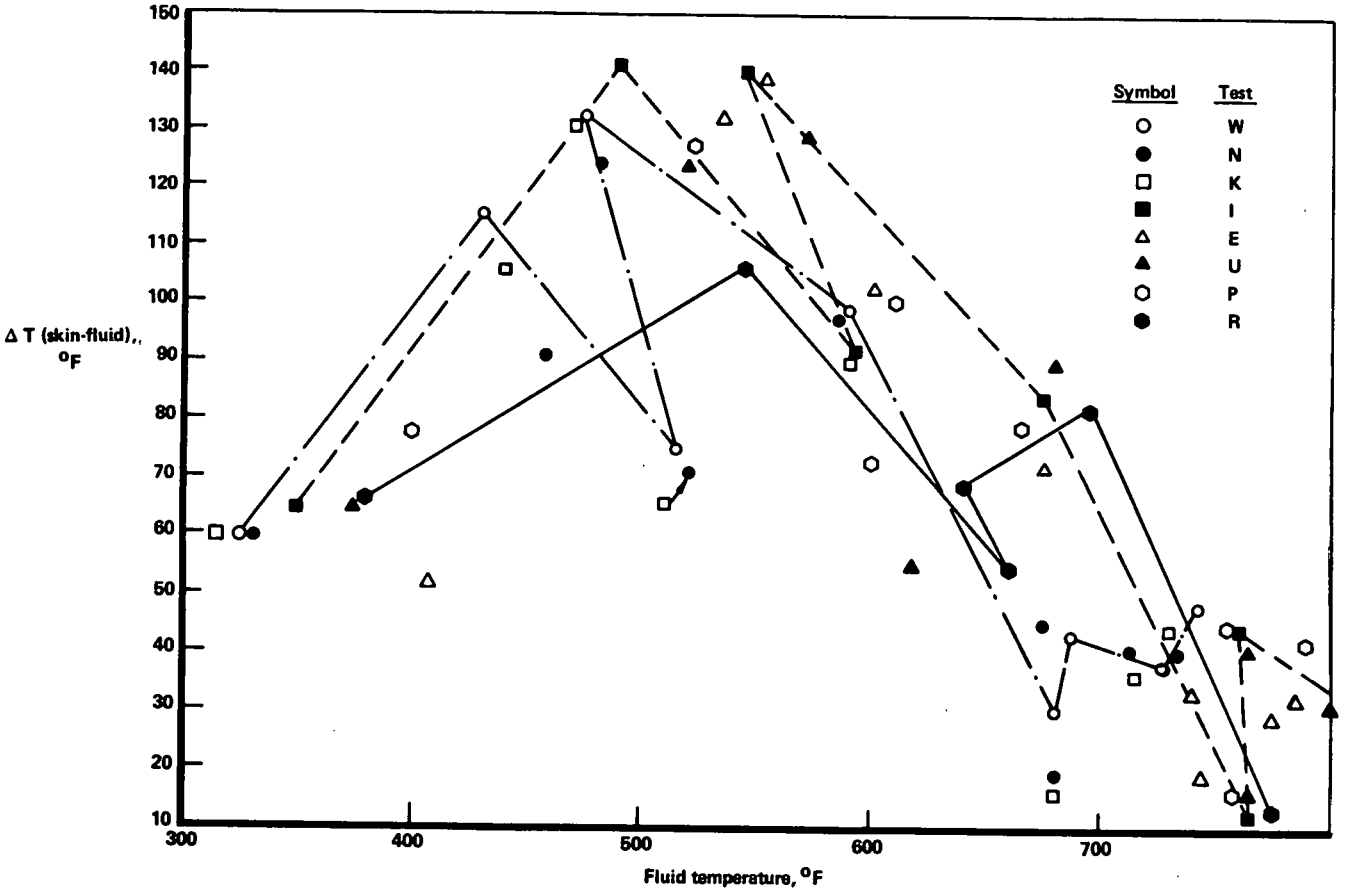

Figure 6
Wilsonville Preheater Test Analyses
Viscosities Determined
By Lockhart — Martinelli Pressure Drop Correlation

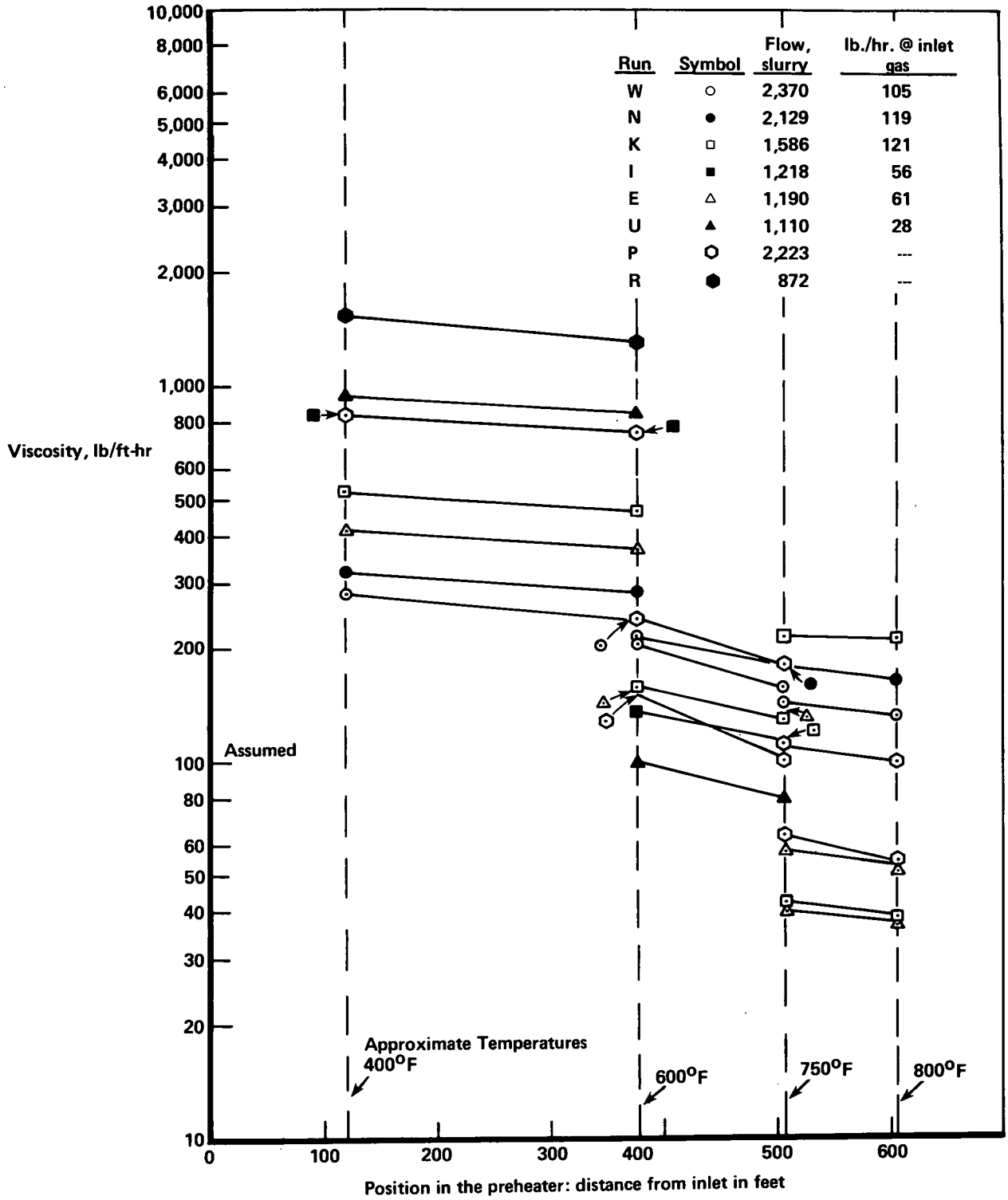

Figure 7
Wilsonville Preheater Test Analyses
Viscosities Determined
By Dukler Constant Slip Pressure Drop Correlation

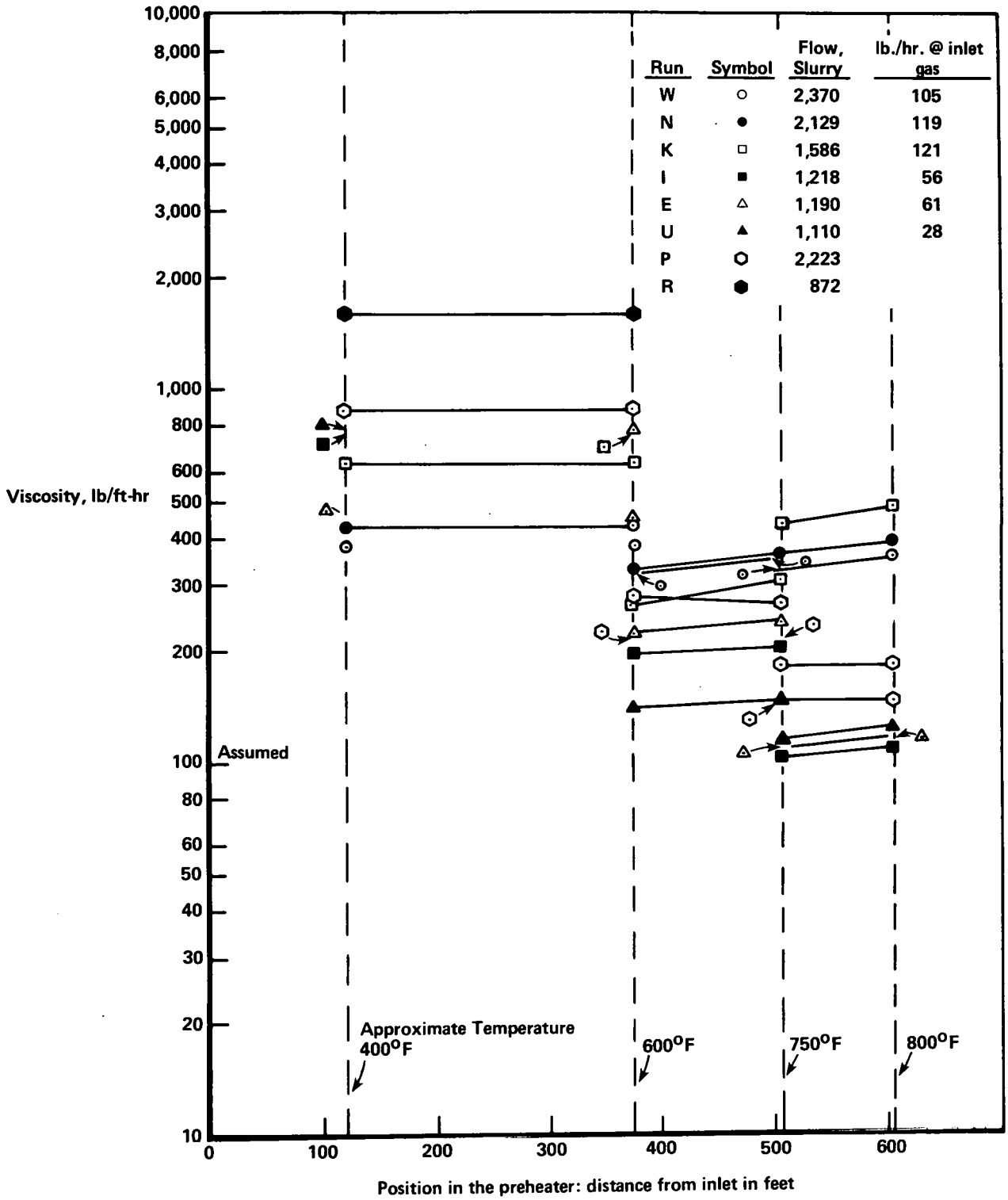

Figure 8
Wilsonville Preheater Test Analyses
Viscosities Determined
By Dukler No-Slip Pressure Drop Correlation

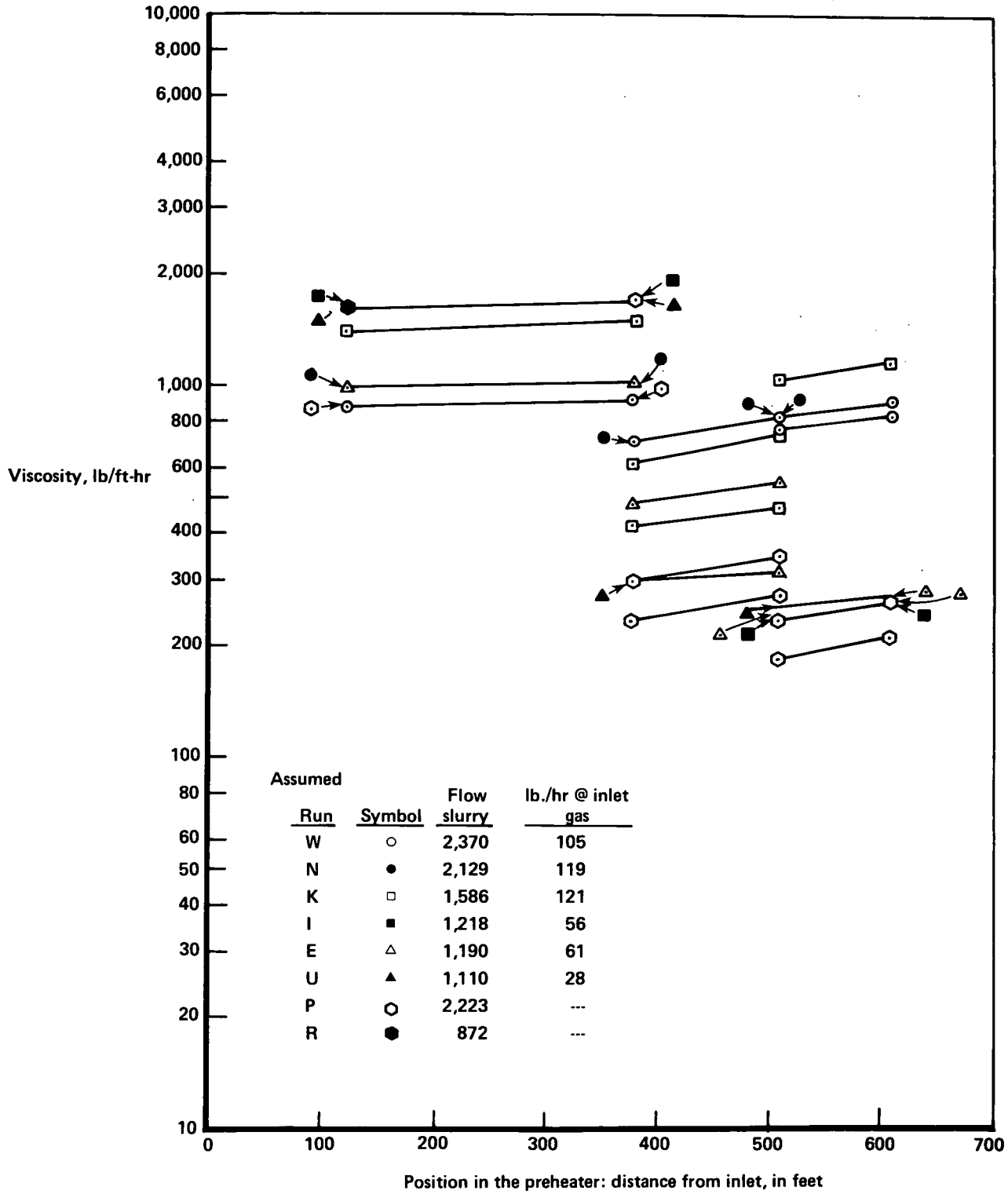

Run	Symbol	Assumed Flow slurry	lb./hr @ inlet gas
W	○	2,370	105
N	●	2,129	119
K	□	1,586	121
I	■	1,218	56
E	△	1,190	61
U	▲	1,110	28
P	⬡	2,223	---
R	⬢	872	---

Figure 9a
Flow Regimes for Wilsonville Test Data Plotted on a Baker Graph

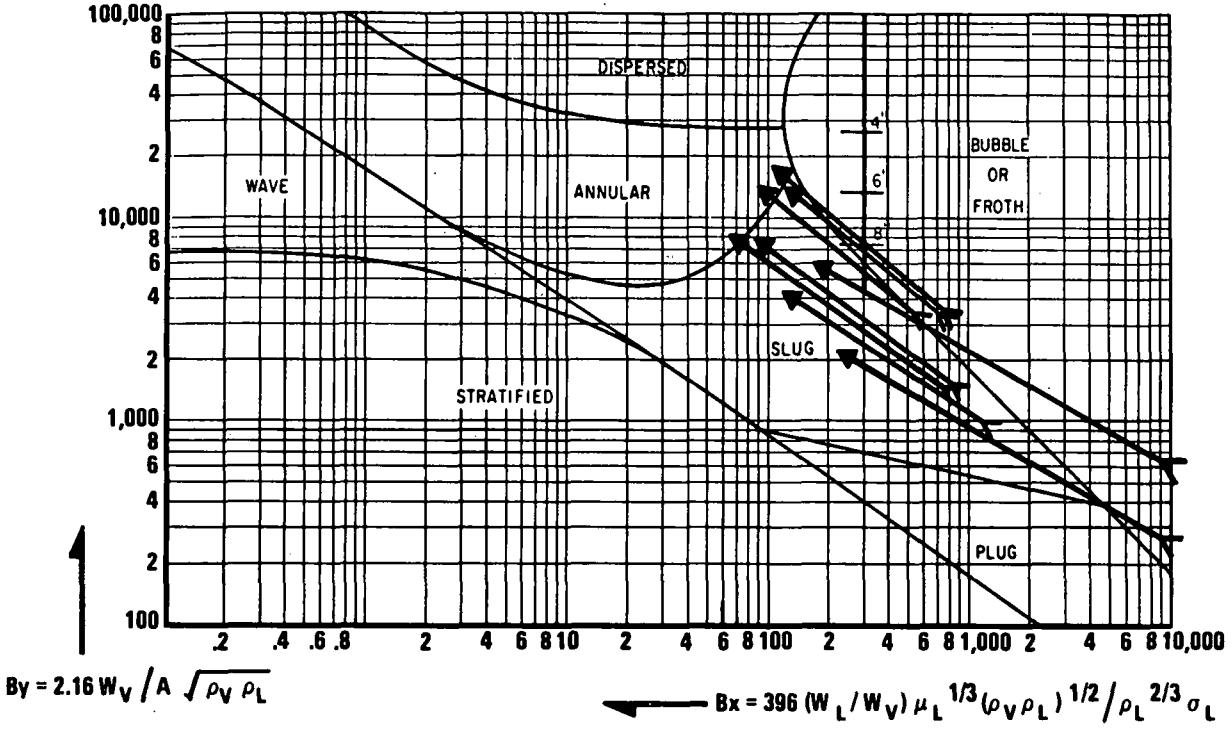

Where: A = Area, ft.^{2}
W_V = Flow rate of vapor, lb./hr.
W_L = Flow rate of liquid, lb./hr.
μ_L = Viscosity of liquid, lb./ft./hr.
ρ_V = Density of vapor, lb./ft.^{3}
ρ_L = Density of liquid, lb./ft.^{3}
σ_L = Surface tension of liquid, dynes/cm

Figure 9b
Flow Regime for Demonstration Plant Plotted on a Baker Graph

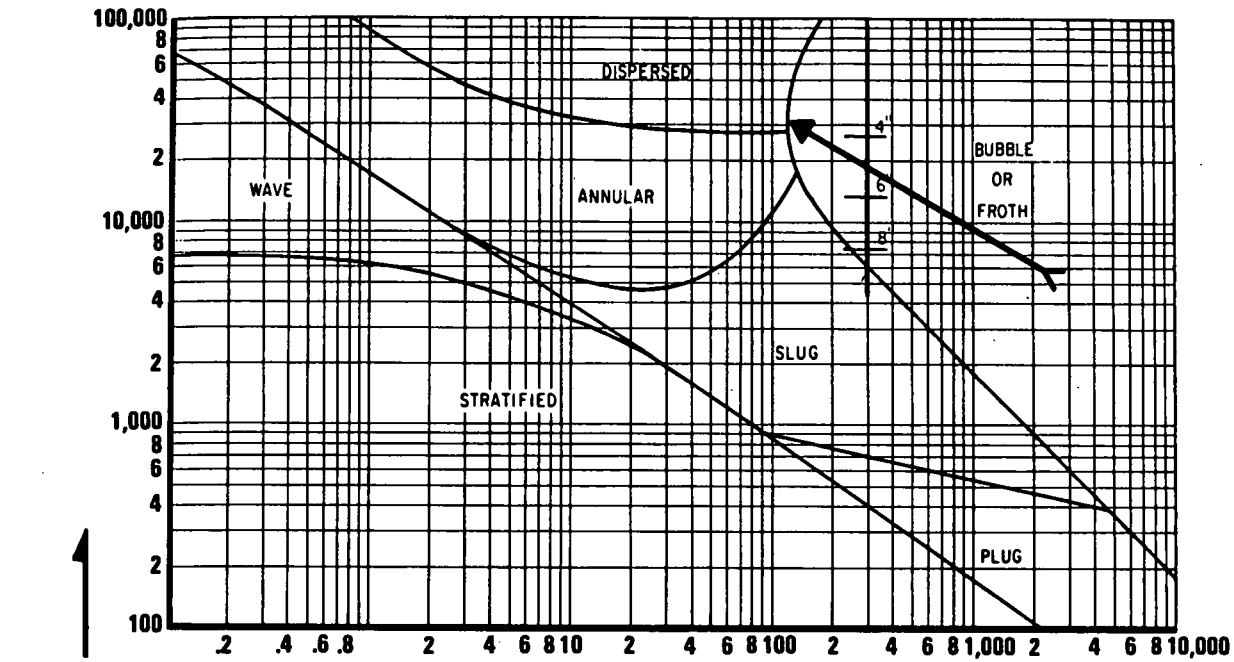

Where: A = Area, ft.^{2}
W_V = Flow rate of vapor, lb./hr.
W_L = Flow rate of liquid, lb./hr.
μ_L = Viscosity of liquid, lb./ft./hr.
ρ_V = Density of vapor, lb./ft.^{3}
ρ_L = Density of liquid, lb./ft.^{3}
σ_L = Surface tension of liquid, dynes/cm

Figure 10
Pump/Slurry Heater Configuration
Phase O Design

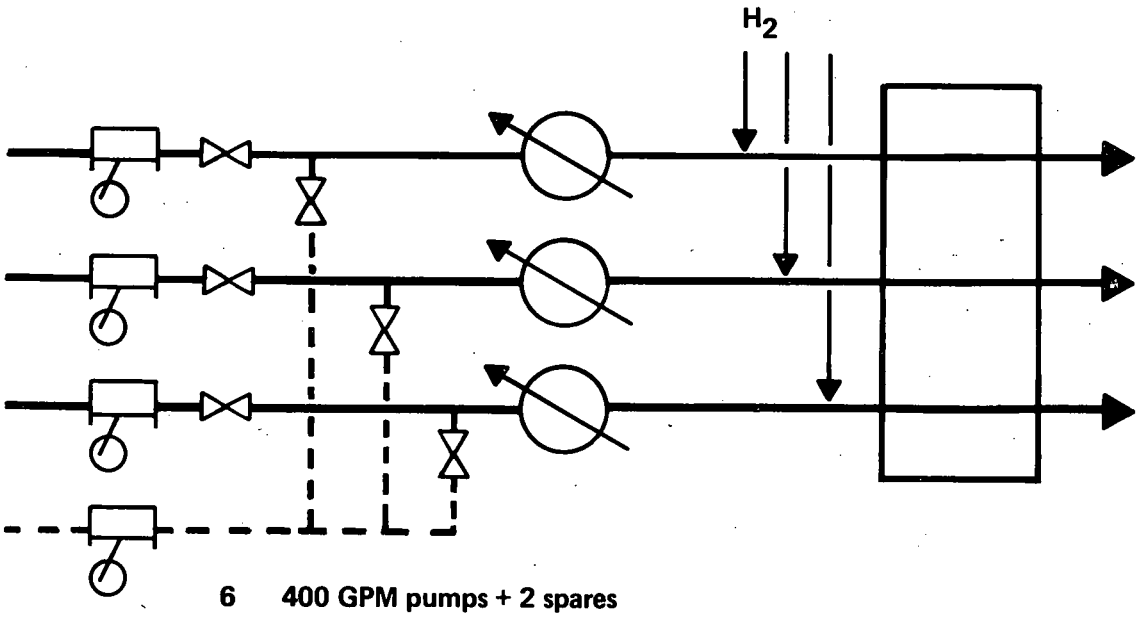

6 400 GPM pumps + 2 spares

6 Sets of heat exchangers

1 Fired heaters 3 X 8 inch dia. tubes. separate circuits.

Figure 11
Pump/Slurry Heater Configuration

Alternative Design A

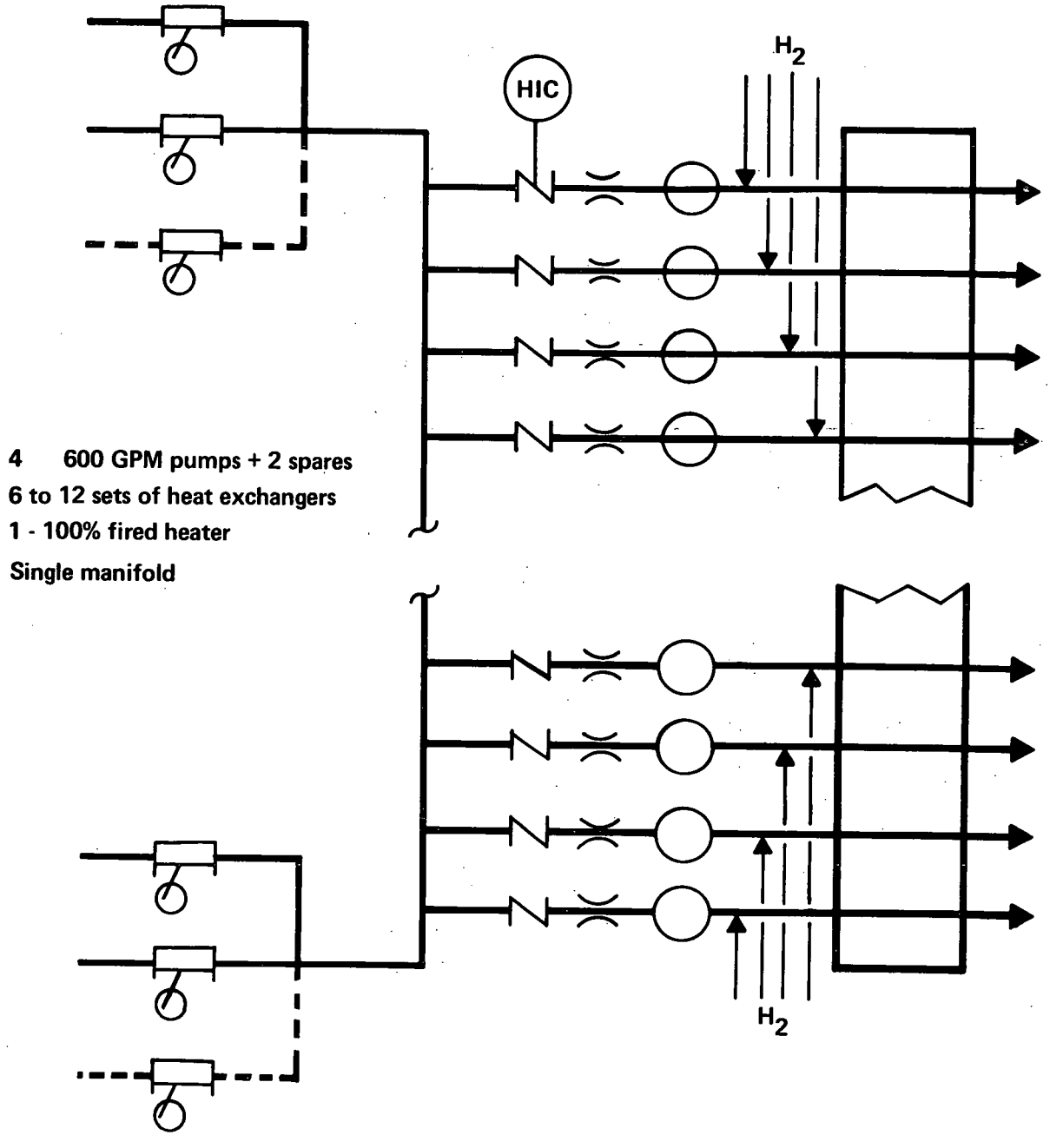

4 600 GPM pumps + 2 spares
6 to 12 sets of heat exchangers
1 - 100% fired heater
Single manifold

Figure 12
Pump/Slurry Heater Configuration

Alternative Design B

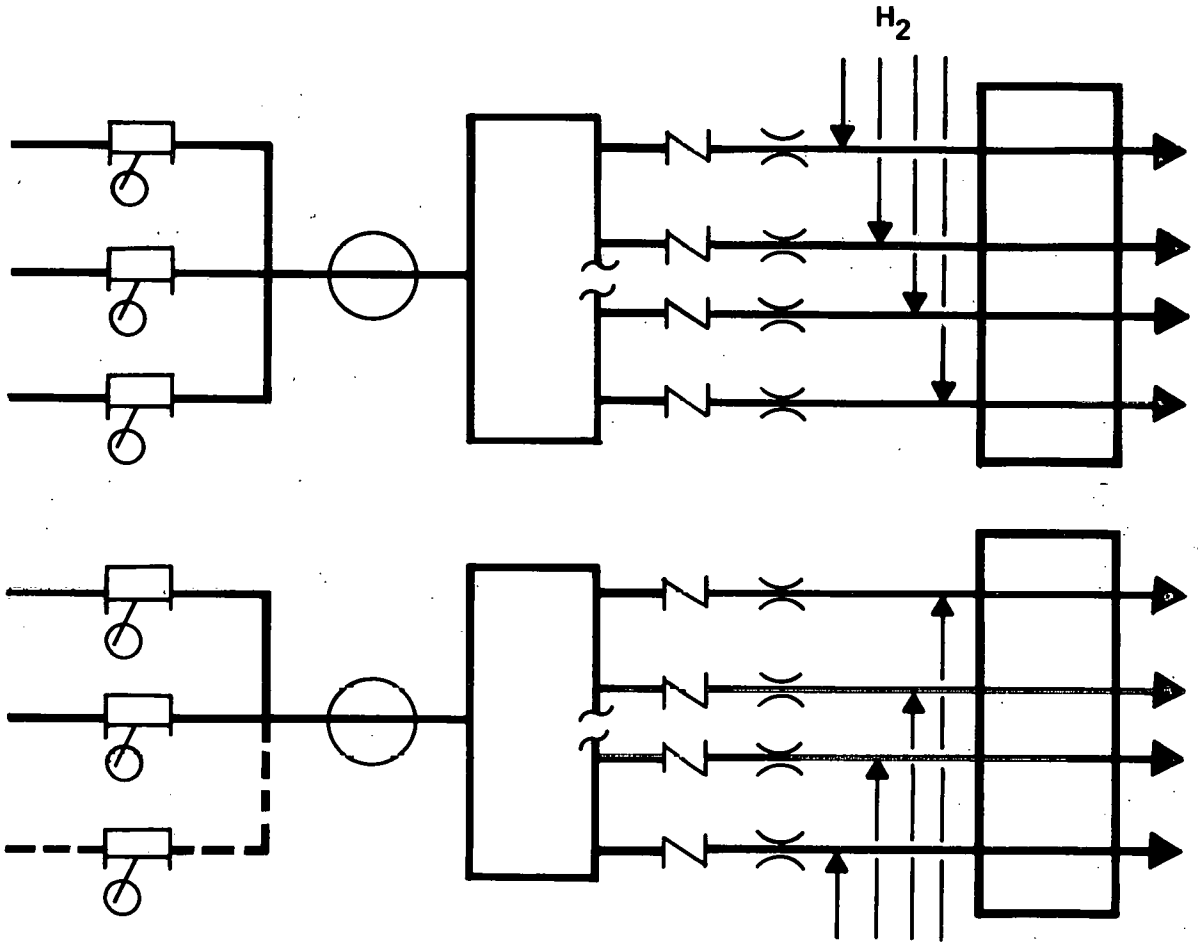

4 600 GPM pumps + 2 spares
2 sets heat exchangers
2 50% fired heaters
2 separate manifolds

A REVIEW OF CURRENT ASSESSMENTS OF THE CO_2 GREENHOUSE EFFECT

Janet A. Firley*

Present climate models predict that, given the projected atmospheric carbon dioxide increases from fossil fuel combustion, the average global temperature will rise 1.5 to 3.0°C near the year 2030.[1] The consequences of this global warming are unknown; they may or may not be favorable.

The projected effects which have a negative environmental impact include:

(1) Dislocation of major agricultural regions due to changing climate and rainfall

(2) Partial melting of the polar ice caps causing 5- to 6-meter rise in sea level[2]

(3) Massive extinction of plant and animal species due to rapid climate change

On the other hand, the positive environmental impacts include:

(1) Longer growing seasons, resulting in increased food productivity

(2) An increase in habitable and food-producing land in the higher latitudes

Not only are the consequences of a given 1.5 to 3.0°C of global warming debatable, the quantitative degree of warming which may be caused by increasing CO_2 is uncertain. Predictions range from a 1.5 to a 4.5°C increase with a doubling of CO_2 levels.[3] In addition to these uncertainties, the amount of CO_2 which will accumulate in the atmosphere due to a given amount of fossil fuel combustion cannot be predicted accurately.

These issues may be resolved as we gain an increased understanding of the climate, the carbon cycle, and the mechanisms and interactions of the carbon reservoirs.

The "Greenhouse Effect"

CO_2 is a gas present in the earth's atmosphere with absorption properties that transmit light energy at wavelengths typical of solar radiation and absorb light energy at wavelengths typical of light reflected by the earth. This phenomenon of trapping solar energy is known as the greenhouse effect.

Today's average CO_2 concentration in the atmosphere is about 334 ppm (parts per million by volume), a one ppm per year increase from the 1958 level of 314 ppm.[4] Fossil fuel combustion is believed to be responsible for the bulk of the CO_2 increase. Therefore, there is growing concern that continued use of fossil fuels as an energy source might further increase atmospheric CO_2 levels and, as a consequence of this increase, the earth's average temperature might rise via the greenhouse effect.

*ICRC

Increase in CO_2

The evidence for increasing atmospheric CO_2 has been well documented since 1958, when the first systematic and accurate observations began. Observations have been recorded (Figure 1) from Swedish aircraft; Point Barrow, Alaska; the Antarctic; and Mauna Loa, Hawaii.[5] These average yearly data indicate that since 1958 CO_2 has been increasing throughout the world at 0.2% to 0.3% per year to the present level of 334 ppm. The earliest record of atmospheric CO_2 concentration was taken between 1898 and 1901 at Kew, England, by Brown and Escombe. The reported mean value was 290 ppm.[6] However, the data is of questionable accuracy.

The most frequent and continuous monitoring is being collected at the Mauna Loa Observatory. These data (Figure 2) show seasonal variations of 5 ppm in CO_2 concentration, due to photosynthesis.[7] Although this monitoring is continuous, many observations are made three times a month, at noon, when turbulence has reduced local effects to a minimum.

Local effects are those from industrial combustion processes or photosynthetic activity of plants. Photosynthesis, the process which consumes CO_2 to form organic compounds, can cause a daily variation in CO_2 concentration of 160 ppm, as shown in Figure 3.[8] This sampling was done at 1, 4.5, and 22.5 meters above a wheat field. The lowest value (310 ppm) was reached before sunset and the highest value (470 ppm) was reached at sunrise. Although local effects are common, the concentration of CO_2 is constant at altitudes greater than a few meters in the troposphere (layer 0-10 miles from the earth's surface) and it remains constant at altitudes extending into the stratosphere (layer 10-25 miles from the earth's surface). A constant mixing ratio has been observed up to 30 kilometers (18 miles or 98,000 feet).[9]

Decrease in Average Global Temperatures

Contradicting the predicted CO_2-induced warming is the decreasing temperature of the earth over the past 40 years. Since 1940, the atmospheric CO_2 has increased more than 20 ppm, yet the earth's average global temperature has decreased 0.5°C during that period.[10] Surface temperature records have been compiled for large portions of the globe for the past 100 years (Figure 4).[11] Slightly less than 1°C variation is observed, indicating that presently either the earth's temperature is somewhat stable or that temperature changes on the order of several degrees are occurring at very slow rates.

Geological evidence suggests that the global average temperature has not varied outside the 7 to 27°C range and that the average global temperature during the last major ice age (10,000 years ago) was only about 3°C lower than it is today.[12] We are presently in a warm era; the average global temperature of the past 10,000 years, 15°C, is approximately 2°C above the believed 850,000-year historical average of 13°C.[13]

The reasons for variations in the earth's temperature are not fully understood. Internal forces, such as the interaction of the land, ocean, atmosphere, and ice system, may alone determine climate. Or they may not—and external causes of climate variation may include volcanic dust, sun spots, and human-induced changes in CO_2, aerosols, particulates, and heat. Of the external causes, only volcanic dust shows any high degree of correlation with climate observations of the past 100 years. Particulate matter discharged to the atmosphere from volcanic eruptions blocks solar radiation, thereby decreasing the average global temperature. Records of volcanic activity show 80% to 90% correlation coefficients with tem-

perature observations.[14] In the same study, human-induced causes resulted in small magnitude changes in temperature which cancelled one another; the warming effect, due to added CO_2 and heat, cancelled the cooling effect, due to added aerosol and particulates.

Although it appears that the atmospheric CO_2 level did not have a significant influence on the earth's temperature variations from 1880 until today, the increased levels of CO_2 predicted by some studies may cause noticeable temperature increases in the future.

The Carbon Cycle

The level to which the atmospheric CO_2 will accumulate in any given year cannot be predicted accurately. This is mainly because we do not understand the mechanisms by which CO_2 enters and leaves the atmosphere. This movement of carbon on earth is known as the "carbon cycle." It is believed that the amount of CO_2 in the atmosphere is determined by some balance between the sources and sinks. Both sources and sinks have been identified, but the dynamic balance between them is unknown (Figure 5).[15]

Sources of atmospheric CO_2 can be classified as "natural" or "manmade." A natural source, probably the largest, is the ocean. About 100 billion tons of carbon enter the air yearly from the ocean in the form of CO_2.[16] Other natural sources of atmospheric carbon dioxide include plant decay and volcanic gases. Man-made sources include fossil fuel combustion, deforestation, and cement manufacture. Approximately 5 billion tons of carbon enter the air yearly in the form of CO_2 from fossil fuel combustion, the largest man-made source.[17]

The sinks for atmospheric CO_2 are natural. The major sinks are the ocean and plants. Estimates for the yearly uptake of carbon as CO_2 are: 100 billion tons to the ocean and 56 billion tons to the plants.[18] The accumulations of carbon (as CO_2 or other compounds) in the sinks eventually enter the large reservoirs of carbon. These reservoirs are deposits of stable carbon containing compounds formed from fixing carbon from the CO_2 as a hydrocarbon, or some other stable carbon compound. The large carbon reservoirs are noncarbonate, such as coal, shale and oil deposits, and carbonate, such as limestone and marble. These reservoirs are estimated to contain about 12,000 billion tons of carbon in the noncarbonate reservoirs and 53,000,000 billion tons of carbon in the carbonate reservoirs.[19]

Through combustion of coal and oil, man is moving carbon from a stable reservoir into the atmosphere and the sinks. As a sink becomes increasingly concentrated with carbon, its properties may change so much that it can no longer support life.

Recently, many researchers have begun to study the carbon cycle and have attempted to quantify the movement (flux) of carbon from one sink to another (see discussion of these studies below). These quantities are not easily obtained and there is a great deal of uncertainty in any estimate. Through an understanding of these fluxes (the carbon cycle), we may be able to predict the level to which carbon may accumulate in the atmosphere. So far, we have not been able to make these predictions with a great deal of certainty.

In addition to making CO_2 accumulation predictions, these studies are attempting to predict what will happen to the various carbon fluxes as a result of increased levels of atmospheric CO_2. Here again, answers are uncertain.

Predicted Increase in "Man-Made" CO_2

Although we do not know what the eventual outcome of an increased flux of CO_2 to the atmosphere will be, we do know what the trends are in man-controlled emissions of CO_2. The major man-made source of atmospheric CO_2 is fossil fuel combustion. We presently depend on combustion of fossil fuels to supply most of our energy and energy requirements are projected to increase.

Man has been putting CO_2 into the atmosphere through combustion of coal, oil, wood, and other hydrocarbons. Between 1958 and 1978, about 78 billion tons of carbon have been emitted to the atmosphere by fossil fuel combustion.[20] If past energy growth rates continue, the energy demand will grow 4.3% per year, and by the year 2030 the atmospheric CO_2 level will double.[21] This projection is drawn from the observation that over the past 20 years the amount of atmospheric CO_2 increase is equal to 50% of the CO_2 evolved from fossil fuel combustion. This empirical relationship may not accurately describe future atmospheric CO_2 accumulations.

The other large atmospheric CO_2 source of which man has been a controlling factor is the clearing of rain forests and other vegetated areas. The contribution to the atmospheric CO_2 increase by deforestation has not been quantified; estimates range from 40 to 200 billion tons of carbon since early last century.[22] Forests cover about 20% to 30% of the land surface and contain 400 to 1000 billion tons of carbon.[23] Plants act as a sink and a source of CO_2. Through photosynthesis, plants use the carbon from CO_2 to form carbon compounds. On the other hand, through respiration plants release CO_2 to the atmosphere. The net carbon difference shows up as plant tissue. Upon death and decay of the plant, this carbon becomes CO_2. This carbon can also be converted to CO_2 by burning the wood. No projections have been made as to the future trends in deforestation.

Although projections of future fuel combustion can be estimated, the accumulation of atmospheric CO_2 which may result cannot be calculated. An accumulation can be assumed, but the timing cannot be predicted.

National Research Council Findings

A recent evaluation of the CO_2 problem by the National Research Council resulted in the following statement:

> "When it is assumed that the CO_2 content of the atmosphere is doubled and statistical thermal equilibrium is achieved, the more realistic of the modeling efforts predict a global surface warming of between 2°C and 3.5°C, with greater increases at high latitudes. (Average temperature increase of 4°C to 8°C in polar regions.) This range reflects both uncertainties in physical understanding and inaccuracies arising from the need to reduce the mathematical problem to one that can be handled by even the fastest available electronic computers. It is significant, however, that none of the model calculations predict negligible warming . . . We have examined with care all known negative feedback mechanisms, such as increase in low or middle cloud amount, and have concluded that the oversimplifications and inaccuracies in the models are not likely to have vitiated the principal conclusion that there will be appreciable warming. . . We estimate the most probable global warming for a doubling of CO_2 to be near 3°C with a probable error ±1.5°C."[24]

The National Research Council felt that the major uncertainty had to do with the ability of the oceans to transfer heat. The oceans act as a thermal regulator—they warm air in winter and cool it in summer. The standard assumption has been that heat transfer is rapid in the surface layers of the ocean, but that it takes a decade or so until the deep ocean layers reach equilibrium with the temperatures of the atmosphere. If this equilibrium is in reality reached in a shorter time period, the global warming will proceed at a slower rate.

As far as the effects of the global warming are concerned, the Council found:

> "The warming will be accompanied by shifts in the geographical distributions of various climate elements such as temperature, rainfall, evaporation, and soil moisture . . . At present, we cannot simulate accurately the details of regional climate and thus cannot predict the locations and intensities of regional climate changes with confidence."

The time it takes to realize a doubling in atmospheric CO_2 is difficult to predict; yet it is the subject of much discussion, especially among environmentalists and those who determine our energy policy. If we knew that a given fossil fuel consumption would cause a doubling of CO_2 in a certain number of years and if we knew what effects this concentration of CO_2 would have on life and climate, then we would be in a better position to form our long-term energy policy.

Sensitivities of the Projections

The assumptions being made today are based on observations of the last 20 years. During that time, 78 billion tons of carbon were emitted to the atmosphere in the form of CO_2 from combustion of fossil fuels. Coincidentally, the increase in atmospheric carbon was 42 billion tons. The conclusion drawn is that 50% of the CO_2 emitted from fossil fuel combustion remains in the atmosphere. This conclusion does not take into account the fact that several billion tons of carbon were emitted to the atmosphere due to deforestation. This may reduce the 50% figure to 40%—maybe lower.[25] The use of this 50% CO_2 retention figure yields a doubling of atmospheric CO_2 by the year 2030, at a growth rate of fossil fuel combustion of 4.3% per year between now and 2030. If the combustion of fossil fuels were to remain constant at today's rate, the time for doubling CO_2 will be well into the 22nd century.[26]

The worldwide growth rate of energy demand since 1860 has been fairly constant at 4.3% per year, except for the time during the two world wars and the economic depression of the 1930s.[27]

By assuming a constant annual growth rate, the energy demand becomes exponential; consequently, the fossil fuel combustion follows, thereby yielding a doubling as the exponential curve steepens. Even at a 2% annual growth rate, the CO_2 doubling will occur around 2060. Indeed, the time of CO_2 doubling does not change much with any reasonable exponential energy demand scenario. Even by changing the 50% CO_2 retention figure to 10% or 1% while assuming 4.3% annual growth of energy demand, the time of doubling becomes 2080 and 2110, respectively. This indicates that under the current assumptions, the doubling is primarily a function of the exponential energy demand.

The energy demand can be met by a means other than combustion of fossil fuels. The alternatives include nuclear, solar, wind, and geothermal. These alternatives currently have other environmental and technical difficulties which are not characteristic of fossil fuels.

CO_2 Emissions From Combustion of Synthetic Fuels

The CO_2 evolution due to combustion of synthetic hydrocarbon fuels is greater than that of natural hydrocarbons because the energy required to produce them adds to the total CO_2 emission. The additional CO_2 evolution is 40% to 60% greater per unit of energy available (see Table 1).[28] The total CO_2 emission from a commercial solvent refined coal (SRC) facility (30,000 TPD coal feed and assuming the worst emissions case of 100% expanded-bed hydrocracker SRC products), including all emissions due to electrical requirements, is 160 million pounds of CO_2 per day (0.008 billion tons of carbon as CO_2 per year). Although this is a large number, it is only 0.16% of the total annual emissions of CO_2 from fossil fuel combustion. Furthermore, the additional CO_2 emitted, due to burning this amount of SRC, rather than an energy-equivalent amount of coal, represents only 0.06% of the total 5 billion tons of carbon (in the form of CO_2) emitted annually from burning fossil fuels. The daily CO_2 emission from one commercial-sized SRC facility is equivalent to 3% of the total CO_2 evolved daily from U.S. automobile emissions.

If the synthetic fuels supply a large portion of the world's energy requirements, the CO_2 increase would be significant. It would cause the doubling of CO_2 to appear sooner. However, the small portion of total worldwide energy demand which would be supplied by synthetic fuels in the next 20 years renders any additional CO_2 increase relatively unnoticeable.

Current Work

Current work being done on issues which relate to the atmospheric CO_2 buildup is being directed and funded mainly through the Office of Carbon Dioxide Effects Research and Assessment which is part of the Department of Energy. This office, formed in March 1977, is committed to a research program which obtains the best facts and knowledge of the CO_2 issue. Its main thrust at this time is to provide scientific information needed for policy discussions. Forty-four research projects at 30 different institutions are supported by this group. Most of the work concerns climate modeling and study of the carbon cycle. Two major developmental workshops have been held since the program was organized.

The results of studies under this department will be used in forming our future energy policy. In a recent status report, DOE supported the following policy concerning fossil fuel energy:

> "It is premature to implement at this time policy measures which require the reduction in the use of coal or other fossil fuels. We believe the present knowledge is sufficient to require both broad and deep study of many alternative energy supply systems, but does not warrant a policy of curtailment of fossil fuel use. Policies to emphasize the use of coal because of its great abundance in preference to non-fossil (non-CO_2-producing) energy supply systems are equally unjustified."[29]

Summary

The atmospheric CO_2 concentration has been increasing 1 ppm per year for the past 20 years. It will probably continue to increase; the increase may be some direct function of fossil fuel combustion.

If the level of atmosphere CO_2 were to double from what it is today (330 ppm to 660 ppm) while all other climate parameters remained the same, the average global temperature would increase. The degree of temperature increase may be 3°C ± 1.5°C. The warming will be accompanied by shifts in the geographical distribution of temperature, rainfall, evaporation, and soil moisture. The locations and intensities of these changes cannot yet be predicted.

The time at which these changes will occur is not known. Based on the past 20 years of observation—with admittedly incomplete data—the atmospheric CO_2 may double by the year 2030 if worldwide energy demand continues to grow about 4% annually and is met primarily by fossil fuel combustion.

Large-scale use of non-fossil fuel energy may delay the CO_2 doubling, while large-scale use of synthetic fuels may hasten the CO_2 doubling.

References

1. *A Comprehensive Plan for Carbon Dioxide Effects Research and Assessment, Part 1: The Global Carbon Cycle and Climate Effects of Increasing Carbon Dioxide*, U.S. Department of Energy, Office of Carbon Dioxide Effects Research and Assessment, Washington, D.C. (May 1979), p. 1.
2. W. P. Elliot and L. Machta (editors), *Workshop on the Global Effects of Carbon Dioxide from Fossil Fuels*, CONF-770385, U.S. Department of Energy, Washington, D.C. (May 1979), p. 107.
3. *Carbon Dioxide and Climate: A Scientific Assessment*, report of an Ad Hoc Study Group on Carbon Dioxide and Climate, National Academy of Sciences, Washington, D.C. (1979), p. 16.
4. Ibid, p. 4.
5. *Man's Impact on the Global Environment: Assessment and Recommendations for Action*, SCEP, Massachusetts Institute of Technology, the MIT Press, Cambridge, Mass. (1979), p. 47.
6. Charles D. Keeling, "Atmospheric Carbon Dioxide in the 19th Century," *Science*, Vol. 202 (8 December 1978), p. 1109.
7. *Summary of the Carbon Dioxide Effects Research and Assessment Program*, U.S. Department of Energy, Office of Carbon Dioxide Effects Research and Assessment, Washington, D.C. (August 1979).
8. Christian E. Junge, *Air Chemistry and Radioactivity*, Academic Press Inc., New York (1963), p. 23.
9. Ibid, p. 92.
10. Alan Robock, "Internally and Externally Caused Climate Change," *Journal of the Atmospheric Sciences*, Vol. 35 (June 1978) p. 1111.
11. Ibid, p. 1112.
12. Elliot and Machta, *Workshop on Global Effects of Carbon Dioxide*, pp. 91-93.
13. Ibid, p. 92.

14. Robock, "Internally and Externally Caused Climate Change," pp. 1116-1121.
15. Bert Bolin, "The Carbon Cycle," *Scientific American*, Vol. 223, Number 3 (September 1970), p. 130.
16. Bert Bolin et al., *The Global Carbon Cycle*, SCOPE 13, John Wiley & Sons, New York (1979) p. 5.
17. Ibid.
18. Ibid.
19. Ibid, p. 343.
20. *Carbon Dioxide and Climate: A Scientific Assessment*, pp. 1-2.
21. Elliot and Machta, *Workshop on the Global Effects of Carbon Dioxide*, pp. 36-40.
22. Bolin, *The Global Carbon Cycle*, p. 49.
23. Ibid, p. 5.
24. *Carbon Dioxide and Climate: A Scientific Assessment,* pp. 1-2.
25. Ibid, p. 5.
26. Ibid, p. 6.
27. Elliot and Machta, *Workshop on the Global Effects of Carbon Dioxide*, p. 37.
28. Janet Firley, "CO_2 Emissions—A Comparison of Fuels," Air Products/Wheelabrator-Frye Joint Venture internal memorandum (20 February 1980).
29. "Working Group III: The Interaction Between Energy Strategies and the CO_2 Question," J. Williams (editor), *Carbon Dioxide, Climate and Society* Proceedings of an IIASA Workshop cosponsored by WMO, UNEP, and SCOPE (21-24 February 1978), p. 316.

Table 1

Comparison of CO_2 Emissions From Natural and Synthetic Fossil Fuels

Basis: 1 MM Btu available energy; no emission control equipment on end use combustion (i.e., scrubbers, precipitators, bag houses)

Fuel	Fuel required (lb)	CO_2 emission (lb)	Emission ratio CO_2 fuel/CO_2 coal
Coal	78.4 (coal)	203	1.00
SRC	63.3 (SRC)	202	1.00
SRC + processing	113 (coal)*	291	1.43
Expanded-bed hydrocracker SRC + processing	128 (coal)*	333	1.64
Natural gas	41.9 (NG)	115	0.57
#6 fuel oil	58.2 (oil)	183	0.90

*Coal requirement includes that which is necessary for the process and for the electricity; electricity supplied by a 35% efficient electrical utility fueled by SRC.

Figure 1
Annual Mean Values of CO_2

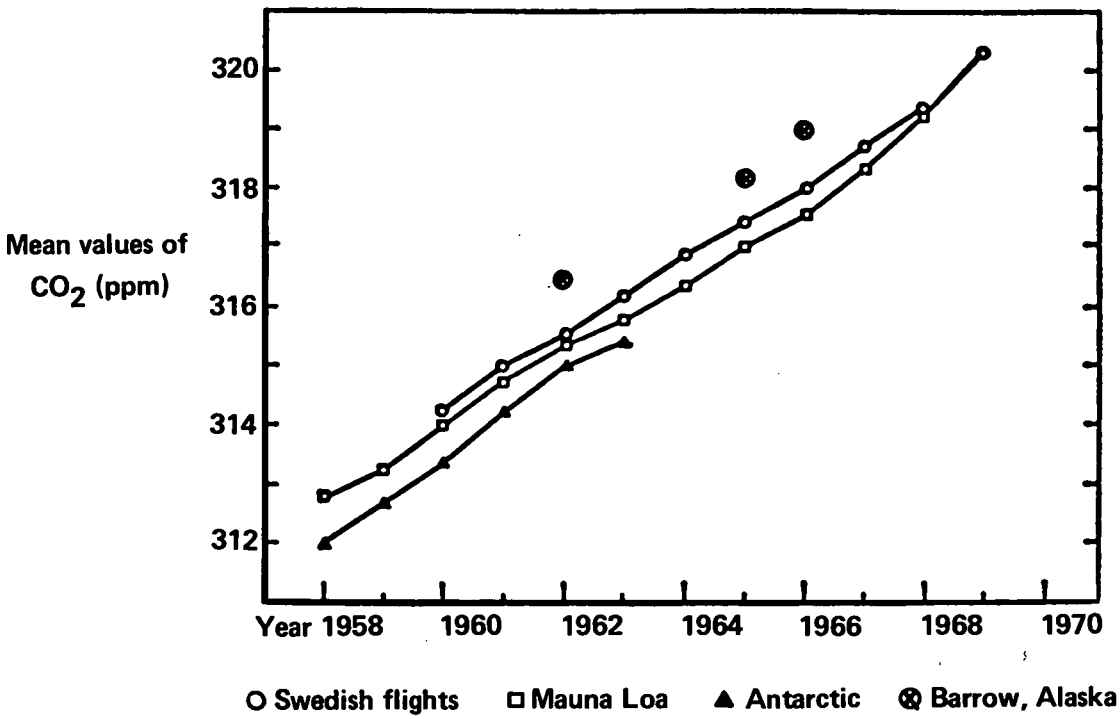

Sources: Swedish flights (Bolin and Bischof, 1969); Mauna Loa (Pales and Keeling, 1965, Bainbridge, 1970); Antarctic (Brown and Keeling, 1965); Barrow, Alaska (Kelley, 1969)

Figure 2
Mean Monthly Carbon Dioxide Concentrations at Mauna Loa, Hawaii

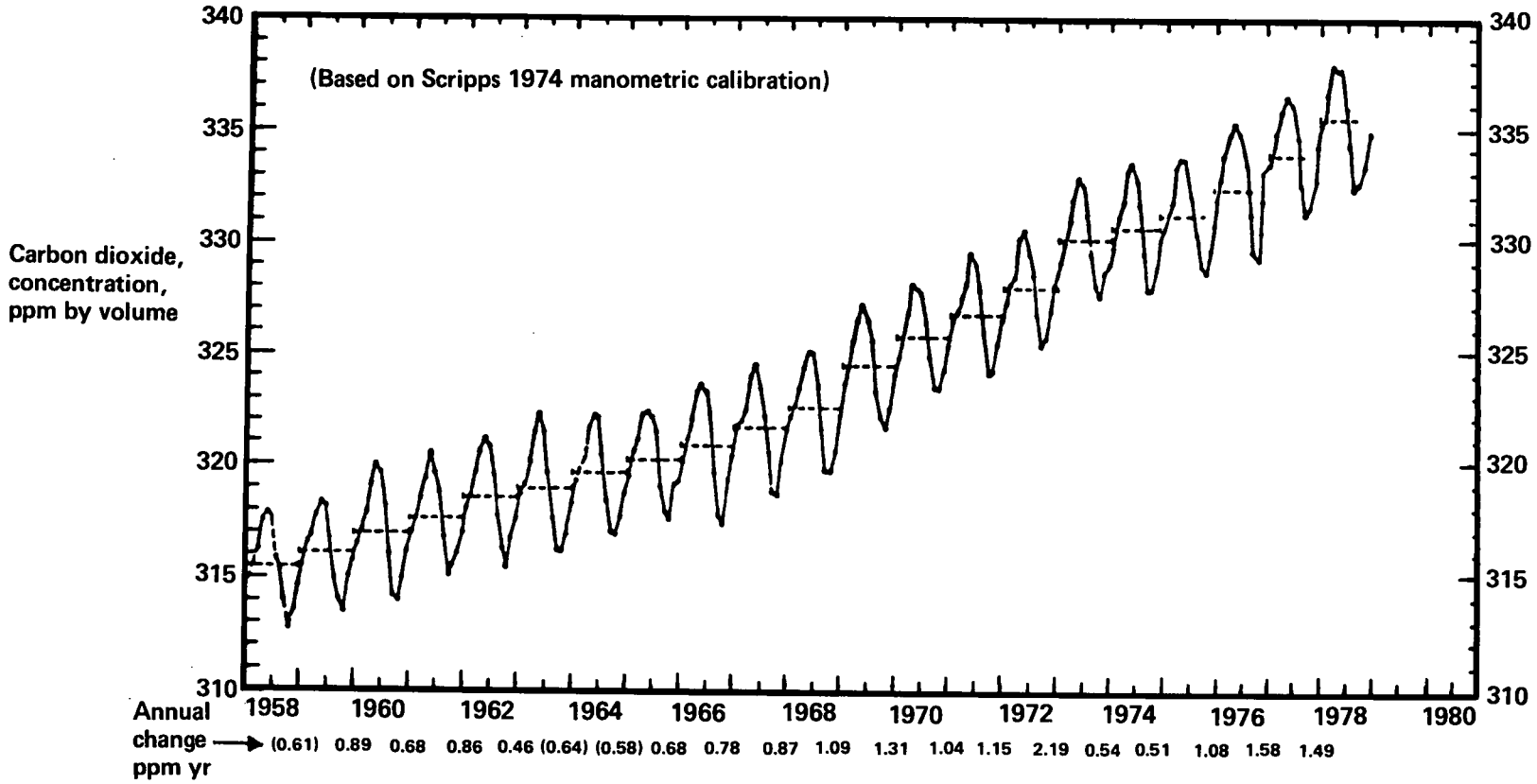

Source: Keeling, 1976 (updated by MACHTA)

Figure 3
Daily Variation of CO_2 at 1, 4.5, and 22.5 Meters Above a Wheat Field

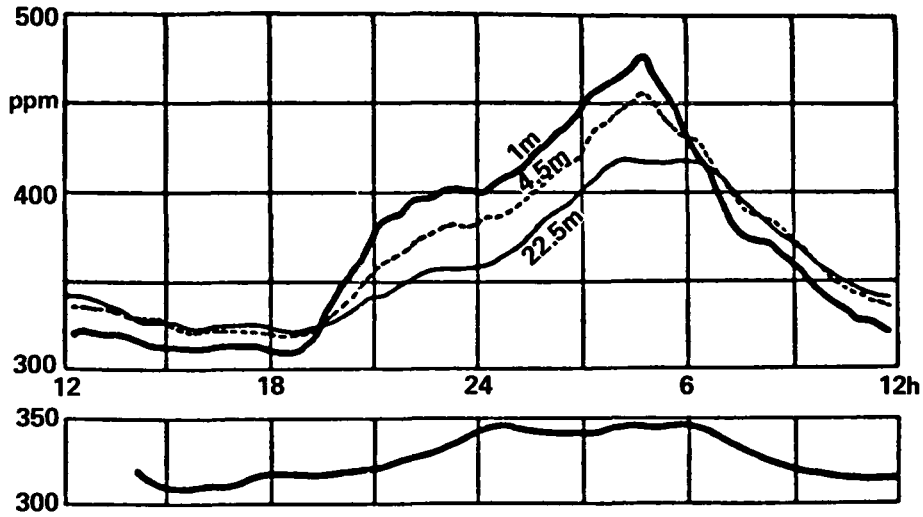

Taken during sunny weather (upper) and overcast weather (lower). In the latter case, the difference between the three heights was too small to be plotted.

Source: Huber, 1952

Figure 4
Annual Mean Temperature of the Northern Hemisphere for 1881-1975

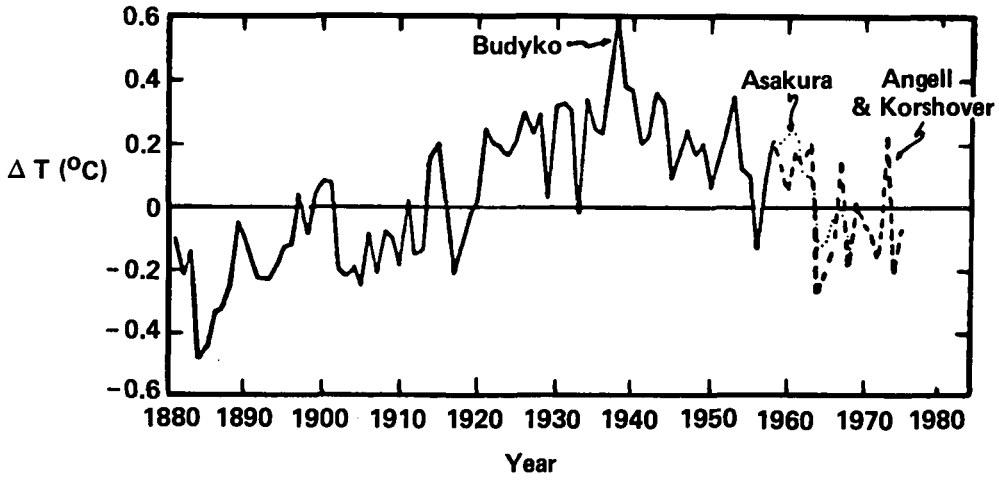

Sources: Budyko (1969), Asakura (Gates & Mintz, 1975) and Angell and Korshover (1977)

Figure 5

The Carbon Cycle As Estimated By B. Bolin (1970).

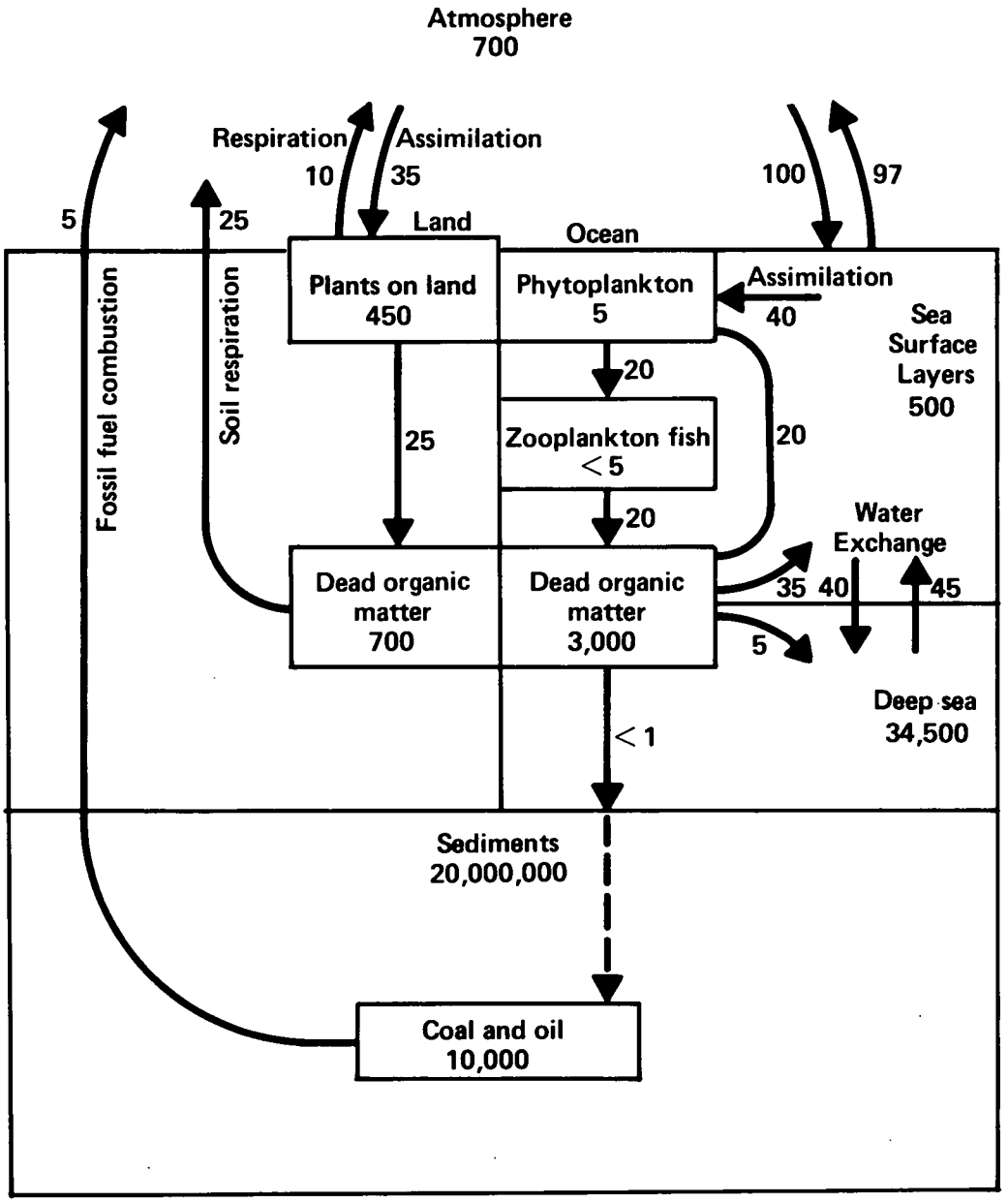

POSTSCRIPT ON METHODOLOGY: 8-HOUR SEPARATION PROCEDURE

F. K. Schweighardt*

In a typical liquefaction process preasphaltenes are generated in the dissolver stage with only small quantities of hydrogen consumed. Physical changes occur; the concentration of slurry solids decreases, the viscosity increases, and some thermal effects are noticed.

In the reaction zone downstream (or still in the dissolver if recycle solvent and hydrogen conditions are sufficient), asphaltenes, benzene-solubles, and pentane-insolubles increase. Depending upon residence time, pentane-soluble oils may be generated along with hydrocarbon gases. As the process stream travels along, it sees a multitude of conditions, including regressive reactions in which these products revert to less soluble components. Many of these regressive reactions seem to produce pyridine-insoluble components similar to the original coal—but much less reactive.

Because of the complexity of coal-derived products, some degree of separation is required in order to classify and quantify changes occurring during conversion. The separation technique used in the Corporate Laboratories of Air Products and Chemicals, Inc. (APCI) isolates oils, asphaltenes, preasphaltenes, and residue in a matter of eight man-hours.

The procedure applies classical coal chemistry thought to present state-of-the-art technology. The philosophy is to define each subfraction in terms of *solubility in* and not as a *precipitate from* a particular solvent or solvent pair.

A sample of the total product stream from a process unit (100 ml) is obtained at the appropriate letdown stage (and held at 4°C under a nitrogen blanket if a delay in analysis is anticipated). The sample is warmed to 50°C and sonicated (20 MHz at 200 watts) for 10 minutes to regenerate a homogeneous prime sample. A five-gram sample is removed for determination of elemental composition and ash; a second five-gram analytical sample is then solvent-separated. The analytical sample (5 g ± 0.005) is frozen in liquid nitrogen, ground to a coarse powder (100%-100 mesh), then quickly diluted with n-pentane (100 ml) and sonicated to initially extract the pentane-soluble oils.

The pentane-sonication-extraction regime is repeated three times with each supernatant being decanted into a Millipore stainless steel pressure filter containing a 5-micron fluoropore filter element. A fourth and fifth wash (100 ml) is used to decant all remaining solids into the filter unit. Nitrogen gas is used to inert the sample and force the solubles through the filter for collection. While the filtrate is purged with dry nitrogen, the solvent volume is reduced at 50°C on a Rotovapour-R. Pentane extraction (2 liters) is continued until just a faint yellow color remains.

*Air Products and Chemicals, Inc.

Benzene is next used to continue the extraction to recover the asphaltenes in a similar fashion as pentane. Nearly two liters of benzene are required. Pyridine (2-2.5 liters) is the final solvent for extraction to reclaim the preasphaltenes. This procedure leaves the residue (mineral matter and insoluble organics) on the filter. After back-washing with methanol and methylene chloride to remove residual pyridine from the wet residue, it is dried *in situ* with nitrogen, and then removed and weighed to quantify the residue weight percent.

Solvents other than pentane have been used: hexanes, heptane, and cyclohexane. Each gives (in the order cited) slightly more oils and therefore fewer asphaltenes, without greatly affecting the quantity of preasphaltenes or residue. Toluene has been substituted for benzene without major problems, except that the laboratory workup time is extended and some product changes may occur due to prolonged heating. Residual benzene on the other hand is removed from the asphaltene solution by sublimation at 4°C under 1-5 mm Hg in one to two hours. Ethyl acetate has been used recently to isolate asphaltenes, but with mixed results due to poor solvent removal.

As for the preasphaltenes, tetrahydrofuran (THF) has been substituted for pyridine, but the instability of ethers without peroxide inhibitors (e.g., butyl hydroxytoluene, BHT) provides an unsafe working environment. Methylene chloride with methanol (9:1) has been used with good success, but this mixture recovers only 80-90% of the pyridine solubles—an error that could well influence kinetic measurements in which coal-to-preasphaltene data is most important.

This methodology requires one laboratory assistant eight hours to complete, excluding cleanup and writing the report. To demonstrate the effectiveness of the method, the average material recovery has been 98% and the elemental balances have been within experimental error limits (±0.3%). Experience with the method reduces errors.

For example, a total product from a Coal Process Development Unit run was analyzed and solvent-separated as follows:

Sample name	Material balance							
	wt % recovery	C	H	O[1]	N	S	Ash	$\bar{n}$MW[2]
Product	—	76.8	6.9	3.7	1.2	1.4	9.9	300
	(weighted elemental composition)							
Oils[3]	57.5	50.3	5.1	1.3	0.4	0.4	—	200
Asphaltenes	11.9	10.1	0.8	0.6	0.2	0.2	—	400
Preasphaltenes	14.2	11.8	0.8	0.9	0.4	0.2	—	900
Residue	16.4	4.4	0.3	0.7	0.1	0.7	10.2	—
Totals	98.4[3]	76.6	7.1	3.5	1.1	1.5	10.2	—

1. Direct determination.
2. Vapor pressure osmometry, 27°C in methylene chloride, four points extrapolated to infinite dilution to give a number that is the average molecular weight.
3. Material loss adjusted to oils as volatiles removed during workup; 1.6%.

Data on this solvent separation procedure is presently being evaluated.

A different separation procedure is presently being used at the Wilsonville Pilot Plant. Asphaltenes are precipitated from a solvent mixture of pentane and benzene (9:1)—therefore defining the oils as being the soluble portion. Preasphaltenes at Wilsonville are

the creosote solubles of the benzene insolubles after Soxhlet extraction. Losses are not directly accounted for, but distributed among the subfraction.

Here is a comparison of the results obtained by the APCI and the Wilsonville methods, using a sample of full-range SRC (M-61):

Comparison of Solvent Separation Methods

	wt %	
	APCI	**Wilsonville**
Oils	1	16
Asphaltenes	43	25
Preasphaltenes	56	59
Residue	0	0

The major difference is that the oils are apparently 16 times greater from the Wilsonville method—the result of a difference in the definition of oils. The APCI definition considers oils to be those components that are soluble in n-pentane. Wilsonville defines oils as those components soluble in 90% pentane and 10% benzene.

To continue the characterization of the hydrogen donor recycle solvent, APCI has chromatographically separated the oil into functional groups: saturate (paraffin and cyclo-paraffin), aromatic-hydroaromatic, phenolic, and nitrogen bases. For instance, a recent Wilsonville solvent, V131B/190AMB, was separated to give these results:

	wt %
Saturate	18
Aromatic	51
Phenolic	26
N-base	5

Further analyses of the subfractions are under way and will be reported later.

SRC-I QUARTERLY TECHNICAL REPORT DISTRIBUTION

DEPARTMENT OF ENERGY

Mr. J. L. Morris
Mail Stop E-333
Washington, DC 20545

Mr. James Batchelor
Mail Stop E-338
Washington, DC 20545

Mr. R. M. Hamilton
Mail Stop E-333
Washington, DC 20545

Mr. W. S. Jones
Mail Stop E-333
Washington, DC 20545

Mr. R. R. Santore
P.O. Box 364
Catlettsburg, KY 41129

Mr. W. M. Vaden (2)
U.S. Technical Information Center
P.O. Box 62
Oak Ridge, TN 37830

Mr. John Pearson (4)
SRC Project Office
P.O. Box E
Oak Ridge, TN 37830

Mr. Robert Lynch
Contracts Office
P.O. Box E
Oak Ridge, TN 37830

Mr. Robert Poteat
Patent Office
P.O. Box E
Oak Ridge, TN 37830

Mr. H. D. Cochran (2)
Oak Ridge National Laboratory
P.O. Box X
Oak Ridge, TN 37830

KENTUCKY DOE

Mr. John Mitchell
Kentucky Center for Energy Research
Iron Works Road
P.O. Box 11888
Lexington, KY 40578

EPRI

Mr. H. Lebowitz
Electric Power Research Institute
3412 Hillview Avenue
P.O. Box 10412
Palo Alto, CA 94303

UOP/SDC JOINT VENTURE

Mr. O. H. Tallman
P.O. Box 842
Oak Ridge, TN 37830

Exxon Coal Liquefaction Pilot Plant
Carter Oil Company
5011 Baker Road
Baytown, TX 77520

SOUTHERN COMPANY SERVICES, INC.

Mr. E. Huffman
P.O. Box 2625
800 Shades Creek Parkway
Birmingham, AL 35202

PETC

Mr. S. Rodgers
4800 Forbes Avenue
Pittsburgh, PA 15213

PITTSBURGH AND MIDWAY MINING

Mr. John Segerson
Technical Coordinator
Pittsburgh & Midway Mining Co.
P.O. Box 199
Dupont, WA 98327

Mr. John Sobernheim
Engineering Manager
Pittsburgh & Midway Mining Co.
P.O. Box 3396
Englewood, CO 80155

H-COAL PILOT PLANT

Martha K. Hall
Ashland Synthetic Fuels, Inc.
P.O. Box 391
Ashland, KY 41101